PB86-103470

NBS (National Bureau of Standards) Materials Measurements. Annual Report for 1 April 1984-31 March 1985

(U.S.) National Bureau of Standards
Gaithersburg, MD

Prepared for

National Aeronautics and Space Administration
Washington, DC

Jul 85

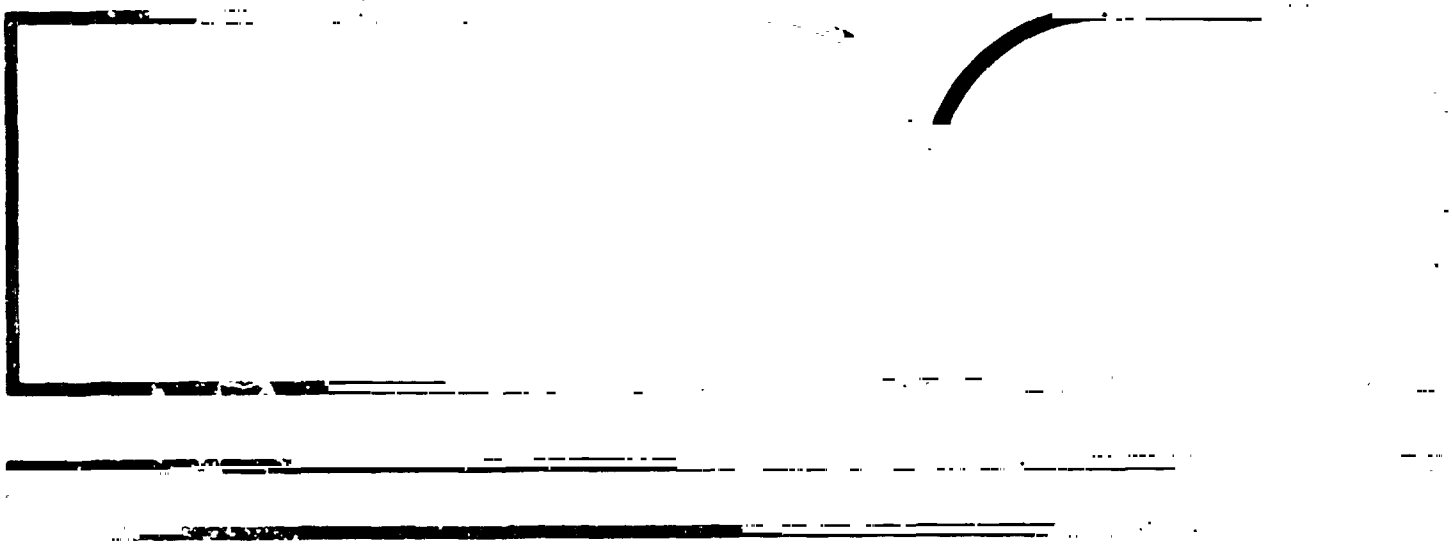

U.S. Department of Commerce
National Technical Information Service
NTIS

NBS-114A (REV. 2-8C)

U.S. DEPT. OF COMM. BIBLIOGRAPHIC DATA SHEET (See instructions)	1. PUBLICATION OR REPORT NO. NBSIR-85/3217	2. Performing Organ. Report No. PB86 103470/AS	3. Publication Date AUGUST 1985

4. TITLE AND SUBTITLE

NBS: Materials Measurements

5. AUTHOR(S)

J. R. Manning

6. PERFORMING ORGANIZATION (If joint or other than NBS, see instructions)

NATIONAL BUREAU OF STANDARDS
DEPARTMENT OF COMMERCE
WASHINGTON, D.C. 20234

7. Contract/Grant No.

H-27954B

Type of Report & Period Covered

Annual Report
April 1, 1984-March 31, 19

9. SPONSORING ORGANIZATION NAME AND COMPLETE ADDRESS (Street, City, State, ZIP)

Microgravity Science and Applications Division
National Aeronautics and Space Administration
Washington, DC 20546

NBS Category No.
NBS-340

10. SUPPLEMENTARY NOTES

[ ] Document describes a computer program; SF-185, FIPS Software Summary, is attached.

11. ABSTRACT (A 200-word or less factual summary of most significant information. If document includes a significant bibliography or literature survey, mention it here)

This report describes NBS work for NASA in support of NASA's Microgravity Science and Applications Program under NASA Government Order H-27954B (Properties of Electronic Materials) covering the period April 1, 1984 to March 31, 1985. This work has been carried out in three independent tasks:

Task 1. Surface Tensions and Their Variations with Temperature and Impurities

Task 2. Convection during Unidirectional Solidification

Task 3. Measurement of High Temperature Thermodynamic Properties

The results for each task are given separately in the body of the report.

12. KEY WORDS (Six to twelve entries; alphabetical order; capitalize only proper names; and separate key words by semicolons)

convection; directional solidification; gallium; levitation calorimetry; silicon; surface tensions; thermodynamic measurements

13. AVAILABILITY

[X] Unlimited

[ ] For Official Distribution. Do Not Release to NTIS

[ ] Order From Superintendent of Documents, U.S. Government Printing Office, Washington, D.C. 20402

[X] Order From National Technical Information Service (NTIS), Springfield, VA. 22161

14. NO. OF PRINTED PAGES

25

15. Price

NBSIR 85-3217

NBS: Materials Measurements

J. R. Manning

U.S. DEPARTMENT OF COMMERCE
National Bureau of Standards
Gaithersburg, MD 20899

July 1985

Annual Report
For the Period 1 April 1984 - 31 March 1985
NASA Government Order H-27954B
Properties of Electronic Materials

U.S. DEPARTMENT OF COMMERCE
NATIONAL BUREAU OF STANDARDS

NBSIR 85-3217

NBS: MATERIALS MEASUREMENTS

J. R. Manning

U.S. DEPARTMENT OF COMMERCE
National Bureau of Standards
Gaithersburg, MD 20899

July 1985

Annual Report
For the Period 1 April 1984 - 31 March 1985
NASA Government Order H-27954B
Properties of Electronic Materials

U.S. DEPARTMENT OF COMMERCE, Malcolm Baldrige, *Secretary*
NATIONAL BUREAU OF STANDARDS, Ernest Ambler, *Director*

TABLE OF CONTENTS

NATIONAL BUREAU OF STANDARDS
MATERIALS MEASUREMENTS

Summary

This report describes NBS work for NASA in support of NASA's Microgravity Science and Applications Program under NASA Government Order H-27954B (Properties of Electronic Materials) covering the period April 1, 1984 to March 31, 1985. This work was carried out in three independent tasks:

Task 1. Surface Tensions and Their Variations with Temperature and Impurities

Task 2. Convection During Unidirectional Solidification

Task 3. Measurement of High Temperature Thermodynamic Properties

The results for each task are given separately in the body of the report.

With the advent of the Space Shuttle and the accompanying availability of space flight opportunities, it may become feasible to exploit the unique microgravity environment of space flight to produce improved materials and improved measurements of important materials properties. Reduction of convection and enhanced capabilities for containerless processing are two advantages frequently cited for materials processing in space. Both of these topics are under investigation in the current work. Tasks 1 and 2 have been concerned with determining how the reduced gravity obtained in space flight can affect convection and solidification processes. Emphasis in Task 3 is on development of levitation and containerless processing techniques which can be applied in space flight to provide thermodynamic measurements of reactive materials.

In materials processing on earth, gravity frequently produces density-driven convection, thereby causing liquids to be stirred as they solidify. This stirring disturbs the quiescent boundary layer at the solidifying

interface and can be very undesirable if nearly perfect crystals are required. For example, it creates interface instabilities, introduces segregation of components, and produces crystal defects in the resulting solid material. These defects and inhomogeneities, which are particularly troublesome in electronic technology and other advanced technical applications, might be avoided in materials produced under microgravity conditions. Different aspects of these convection processes have been of concern in the first two tasks. Surface tension gradients which may be the main source of convection in space flight experiments have been the measurement focus in Task 1; whereas interactions between solidification processes, convection effects, and interface stability, as influenced by gravity and the lack thereof, are under investigation in Task 2.

In Task 1, which has now achieved its major goals, measurements were made of the surface tension of liquid silicon and other materials in order to provide reliable values for the effects that might be produced by Marangoni convection. This completes work on this task. Silicon is one of the most important materials used in electronic technology. Because of the need for a fully defect-free silicon, not readily obtainable under earth-bound conditions where gravity driven convection can be important, silicon is a major candidate material for processing in space. In planning such space processing, it is important to know the dependence of surface tension on temperature and impurities, particularly oxygen. Surface tension gradients produce Marangoni convection and may be the main source of fluid flows which affect solidification processes in space. During the current reporting period, final sessile drop experiments were performed to establish the temperature (T) dependence of the surface tension (γ) of clean liquid silicon and of clean liquid gallium,

a low-melting point material suggested for use in model space flight experiments, in the temperature ranges above their melting points. Reliable values of $d\gamma/dT$ for these materials were obtained.

In Task 2, convective phenomena which arise during directional solidification are being investigated by both theoretical calculations and experiments. Direct measurements of convection and associated solidification effects have been made during directional solidification of succinonitrile containing small amounts of ethanol; and calculations are being made of convection, interface stability and impurity segregation that should be expected during directional solidification. Measurements were made of the effect of a second fluid phase present as droplets or bubbles near a solidification interface. In cooperation with Centre d'Etudes Nucleaire de Grenoble (CENG) of Grenoble, France, studies have been begun which could lead to experiments with the MEPHISTO space-flight directional solidification system. Numerical calculations were made of fluid flows in directional solidification systems with rigid walls. In addition, linear stability calculations have been carried out for Al-Mg and Pb-Sn alloys of interest for experiments being carried out by other investigators and related to materials processing in space.

In Task 3, assistance is being provided to a joint project involving investigators from Rice University (Professor J. Margrave) and General Electric Co. (Dr. R. T. Frost) in which a General Electric electromagnetic levitation device is being used to develop levitation/drop calorimetry techniques having space flight applications. The critical advantage of such containerless processing experiments is the avoidance of specimen contamination that would occur upon contact of a reactive material with container walls during heating and melting. Automated techniques are being developed in the current work both

to provide support to the on-going ground-based experimental effort in levitation calorimetry and also to act as a prototype for flight experiments. As a major part of the current report an analysis is given of considerations needed in selecting space flight experiments in this topic area.

Task 1

Surface Tensions and Their Variations with Temperature and Impurities

S. C. Hardy

SUMMARY

Measurements of the surface tension of liquid silicon as a function of hydrogen pressure were performed to determine if reductions in oxygen activity would alter the surface tension results found previously in measurements done in purified argon. The result supports the belief that oxygen partial pressures were insignificant in our measurements. Thus for clean silicon it is concluded that the surface tension as a function of temperature can be represented by

$$\gamma = 885 - 0.28(T - 1410)$$

where γ is the surface tension in mJ/m^2 and T is the temperature in Celsius degrees.

The surface tension of liquid gallium has been measured using the sessile drop technique in an Auger spectrometer. The samples were cleaned by argon ion sputtering and were free of impurities to the sensitivity of Auger spectroscopy. The surface tension of liquid gallium is found to decrease linearly with increasing temperature and may be represented as

$$\gamma = 708 - .066\ (T - 29.8)$$

where γ is the surface tension in mJ/m^2 and T is the temperature in Celsius degrees.

Introduction

Research activities during the past year involved studies of the surface tensions of silicon and gallium. The work with silicon was a continuation of the program initiated last year; the gallium research had been started several years ago but had been put aside to undertake the silicon studies. The final six months of funding for this project was used to complete these two investigations.

Surface Tension of Liquid Silicon

In the work described in the last report we measured the surface tension of liquid silicon as a function of temperature in purified argon atmospheres. Our measurements indicated that the surface tension of clean silicon as a function of temperature could be represented by the following expression in the temperature range from 1410°C to 1600°C:

$$\gamma = 885 - 0.28(T - 1410) \qquad (1)$$

where γ is the surface tension in mJ/m^2 and T is the temperature in Celsius degrees. These results were in good agreement with a previous measurement at one temperature in pure hydrogen which is evidence that the oxygen partial pressures were low in our work. However, other measurements showed that the surface tension was very sensitive to low concentrations of oxygen. Thus it is possible the results given by equation 1 were affected somewhat by the residual pressure of oxygen.

The major instrumentation development necessary for quantitative study of the variation of silicon surface tension with oxygen partial pressure was not feasible with the funding and time available in this year's contract. We attempted, therefore, to reduce oxygen activity in our system and thus obtain surface tensions higher than those of equation 1 by performing measurements in argon containing 2% hydrogen. We found no increase in the surface tension

over measurements in pure argon. This result supports our belief that the oxygen partial pressures are insignificant in our measurements. High concentrations of hydrogen could not be used because increased heat losses due to the large thermal conductivity of hydrogen made it impossible to reach the silicon melting temperature with the available equipment. A manuscript entitled "The Surface Tension of Liquid Silicon" was prepared and has been accepted for publication in the Journal of Crystal Growth.

Surface Tension of Gallium

The major effort this year has been directed towards completion of our studies of liquid gallium. Although the surface tension of gallium had been studied extensively, there remained significant uncertainties as to its magnitude and temperature dependence. These data are of interest because gallium has been suggested as a model fluid for Marangoni flow experiments. In addition the surface tension is of technological significance in the processing of compound semiconductors involving gallium.

The scatter in the gallium surface tension data is widely attributed to the presence of trace concentrations of surface active impurities in the different measurements. However, no determination of the surface composition was possible in the earlier experiments; the presence of impurities was inferred from the surface tension values. In the present work we have measured the surface tension of liquid gallium using the sessile drop technique in an Auger spectrometer. This instrument permits a direct analysis of the surface composition concurrently with the surface tension measurement and thus provides the surface characterization lacking in earlier work.

There have been seven[1-7] previously reported studies of the surface tension of gallium over a wide temperature range. Three of these studies found nearly

the same non-linear decrease of surface tension with increasing temperature[1,2,3]. Furthermore, some measurements in our laboratory (unpublished) using similar techniques are in approximate agreement with these other observations of non-linear behavior. These data are shown in Figure 1 along with three linear determinations[4,5,6]. (A fourth linear result is significantly lower and cannot be shown on the scale of Figure 1[7].) Although a non-linear temperature variation is often associated with surface active impurities, the agreement of four independent measurements of non-linear behavior suggests some other factor may be causing the curvature in the temperature variation. In addition, most of the non-linear data lies above the linear data in Figure 1. This seems to be inconsistent with a model in which surface active impurities are causing the non-linearity. Thus the data taken as a whole are anomalous.

Experimental

The Auger spectrometer used in this work is a conventional single-pass cylindrical mirror analyzer (CMA) with a coaxial electron gun. The CMA is mounted vertically so that it can be focussed on the surface of a sessile drop located beneath it. Auger data are acquired in an analog mode using first derivative spectral display. The electron beam can be rastered to form a video image of the drop surface. The system is evacuated with sorption and ion pumps to minimize hydrocarbon concentrations. Pressures in the low 10^{-9} torr range are achieved without baking as measured by a nude ionization gauge. An ion gun and gas supply system permit sample cleaning by argon ion sputtering.

The sessile drop is contained in a shallow cylindrical silica cup which stabilizes the drop and imposes a circular cross-section on the drop base. The cup has an inside diameter of 1.27 cm. Its top has been beveled to form a sharp edge at the inside diameter in order to reduce perturbations of the

drop base due to anisotropic wetting of the cup top[8]. The cup is clamped to a simple hot stage mounted on a horizontal manipulator. The pneumatic vibration isolation supports of the stainless steel bell jar are adjusted to level the cup for the surface tension measurements. A stationary W-Rh thermocouple is inserted directly into the sessile drop to measure the temperature and to provide electrical contact during Auger analysis. The thermocouple is withdrawn from the drop prior to surface tension measurements by translating the hot stage. The drop is viewed through two opposing 8" view ports and is photographed in projected light using an f/5.6 enlarging lens with a 190 mm focal length in conjunction with a 4" x 5" camera body. A fine grained film is used which permits analysis of the negatives at 100X.

The gallium used in these measurements is of 99.99999% purity. The samples are prepared in the form of cylindrical slugs by solidification in a plastic tube under alcohol containing some HCl to dissolve surface oxides. After loading of the sample into the cup and evacuation of the system, the temperature of the hot stage is raised slowly to maintain good vacuum conditions. The gallium melts to form a sessile drop and some impurities desorb from the surface as the temperature is increased to about 400°C. The drop is then cooled and examined by rastering the electron beam over the surface and performing an Auger spectral analysis. After this initial heating the surface is found to be covered by a thin oxide layer with high carbon content. This overlayer of impurities is removed from the liquid surface by sputtering with argon ions[9]. Several cycles in which the sample is heated, cooled and sputtered are necessary before the surface is clean. Even after extensive sputtering an occasional small solid impurity island will be seen. After cleaning, the temperature is adjusted to the desired value, the stage translated

to break contact with the thermocouple, and the drop photographed.

Results and Discussion

The photographs of the sessile drops were analyzed on a measuring microscope and surface tensions calculated using the traditional Bashforth-Adams[10] procedure in conjunction with modern drop shape tables. The diameter of the cup provided a convenient length scale and the density data of Koster et al[11] were used in the analysis. Figure 2 shows the surface tension computed for two drops of different mass in a number of experiments. The drops were heated, cooled and sputtered prior to the surface tension measurements in order to obtain a clean surface. Except for the few small solid impurity islands which probably remained after this procedure, the drop surfaces were free of impurities to the sensitivity of Auger spectroscopy (≈1%). The pressure during the surface tension measurements was less than 10^{-7} torr at the highest temperature (≈500°C) and less than 10^{-8} torr at temperatures below 400°C. Linear regression analysis of the data of Figure 2 yields the following relationship for the surface tension of gallium in mJ/m^2:

$$\gamma = 708 - .066\ (T - 29.8) \qquad (2)$$

Here T is the temperature in Celsius degrees.

In comparison with the previous measurements summarized in Figure 1, this result is closest to that of Yatsenko[6] et al who found

$$\gamma = 712 - .0606\ (T - 29.8) \qquad (3)$$

using density data which differs slightly from that used in our calculations. An adjustment of their relationship to the density data we have chosen yields

$$\gamma = 709 - .066\ (T - 29.8) \qquad (4)$$

Thus the surface tension at the melting point and the slope they find are essentially identical to our results. A density adjustment of the other

measurements shown in Figure 1 does not significantly improve the agreement with our values.

The range in melting point surface tensions of the various measurements, excluding the very low result of Konig and Keck[7], is less than 2%. This is reasonable agreement for surface tension measurements using different techniques and conditions. However, the range in temperature coefficients is much larger, the result of Karashaev[4] being about 50% higher than our determination. The melting point surface tension, temperature coefficient and conditions of the various measurements are summarized in Table 1. We cannot identify the cause of the large discrepancy in temperature coefficient found in the measurements.

As discussed above, the non-linear surface tension data of Figure 1 lie above the linear data at high temperatures. We have found a similar behavior for impurity covered surfaces in our measurements. In Figure 3 we show the surface tension as a function of temperature for a drop with a high surface coverage of impurity islands composed for the most part of carbon. The profile of the impurity covered sessile drop appeared perfectly smooth when examined at 100X magnification which suggests the islands were thin. After sputtering to obtain a clean surface the linear data of Figure 2 were obtained. This behavior is indicated by the line in Figure 3. Thus the presence of a high surface coverage of solid impurity islands is associated with a curved surface tension-temperature plot with the island covered surface tension values exceeding those of the clean surface at high temperatures. This is the general character of the nonlinear data of Figure 1. Presumably the surface tensions calculated from a drop with a high density of surface islands are in error due to distortions of the equilibrium drop shape. If this is

correct, it is surprising that the measurements shown in Figure 1 are in good agreement. It suggests similar concentrations of solid island impurities in four independent experiments.

Another empirical observation of an impurity effect is of interest. During the course of this work it was necessary to open the vacuum system for a minor adjustment of a component after a gallium drop had been cleaned by heating and sputtering. Argon was flushed through the bell jar during this procedure. After reevacuation the surface of the drop was found to be covered by a uniform, thin solid oxide layer. The surface tension was measured to be 750 mJ/m^2, which is significantly higher than the melting point value for a clean surface. This observation suggests that previous measurements of anomalously high surface tensions in gallium[12] may be due to the presence of thin solid oxide films which distort the equilibrium shape of the drop.

In conclusion, we have measured the surface tension of gallium sessile drops which are clean to the sensitivity of Auger spectroscopy. The surface tension decreases linearly with increasing temperature with slope -.066 mJ/m^2K. This result is in excellent agreement with one previous measurement, but is significantly smaller in absolute value than some other determinations. High surface coverages of solid impurities were found to generate a non-linear temperature variation of surface tensions, calculated from sessile drop profiles, presumably due to distortions of the equilibrium drop shape. It is also possible for sessile drops whose surfaces are covered with solid layers to give anomalously high calculated surface tensions.

A manuscript entitled "The Surface Tension of Gallium" has been accepted for publication in the Journal of Crystal Growth.

Table 1. Summary of Linear Surface Tension Results

Reference	γ m.p. (mJ/m^2)	$d\gamma/dT$ (mJ/m^2K)	Conditions
Karashaev[4]	718	-.101	static vacuum
Khokonov[5]	715	-.088	static vacuum
Konig[7]	680	-.091	hydrogen
Yatsenko[6]	709	-.066	dynamic vacuum
This work	708	-.066	dynamic vacuum

References

1. V. I. Nizhenko, L. I. Sklyarenko, and V. N. Eremenko, Ukrain. Khim. Zhnr. 6 (1965) 559.

2. A. G. M. Nalgiev and Kh. IIbragimov, Zh. Fiz. Khim. 48 (1974) 1289.

3. O. A. Timofeevicheva and P. P. Pugachevich, Dokl. Akad. Nauk SSR, 134 (1960) 840.

4. A. A. Karashaev, S. N. Zadumkin and A. I. Kukhno, Russ. J. of Phys. Chem. 41, 329 (1967).

5. Kh. B. Khokonov, S. N. Zadumkin, and B. B. Alchagirov, Elektrokhimiya 10 (1974) 911.

6. S. P. Yatsenko, V. I. Kononenko and A. L. Sukhman, High Temp. (USSR) 10 (1975) 55.

7. U. Konig and W. Keck, J. Less-Common Metals, 90 (1983) 299.

8. Yu. V. Naidich, V. N. Eremenko, V. V. Fesenko, M. I. Vasiliu, and L. F. Kirichenko, in "The Role of Surface Phenomena in Metallurgy," editor V. N. Eremenko, New York, Consultants Bureau, 1963.

9. J. Fine, S. C. Hardy and T. D. Andreadis, J. Vacuum Sci. Technol. 18 (1981) 1310.

10. D. W. G. White, Trans. ASM 55 (1962) 757.

11. Van H. Koster, F. Hensel and E. U. Franck, Berichte Der Bunsen Gesellshaft Fuer Physikalische Chemie, 74 (1970) 43.

12. G. J. Abbaschian, J. Less-Common Metals, 40 (1975) 329.

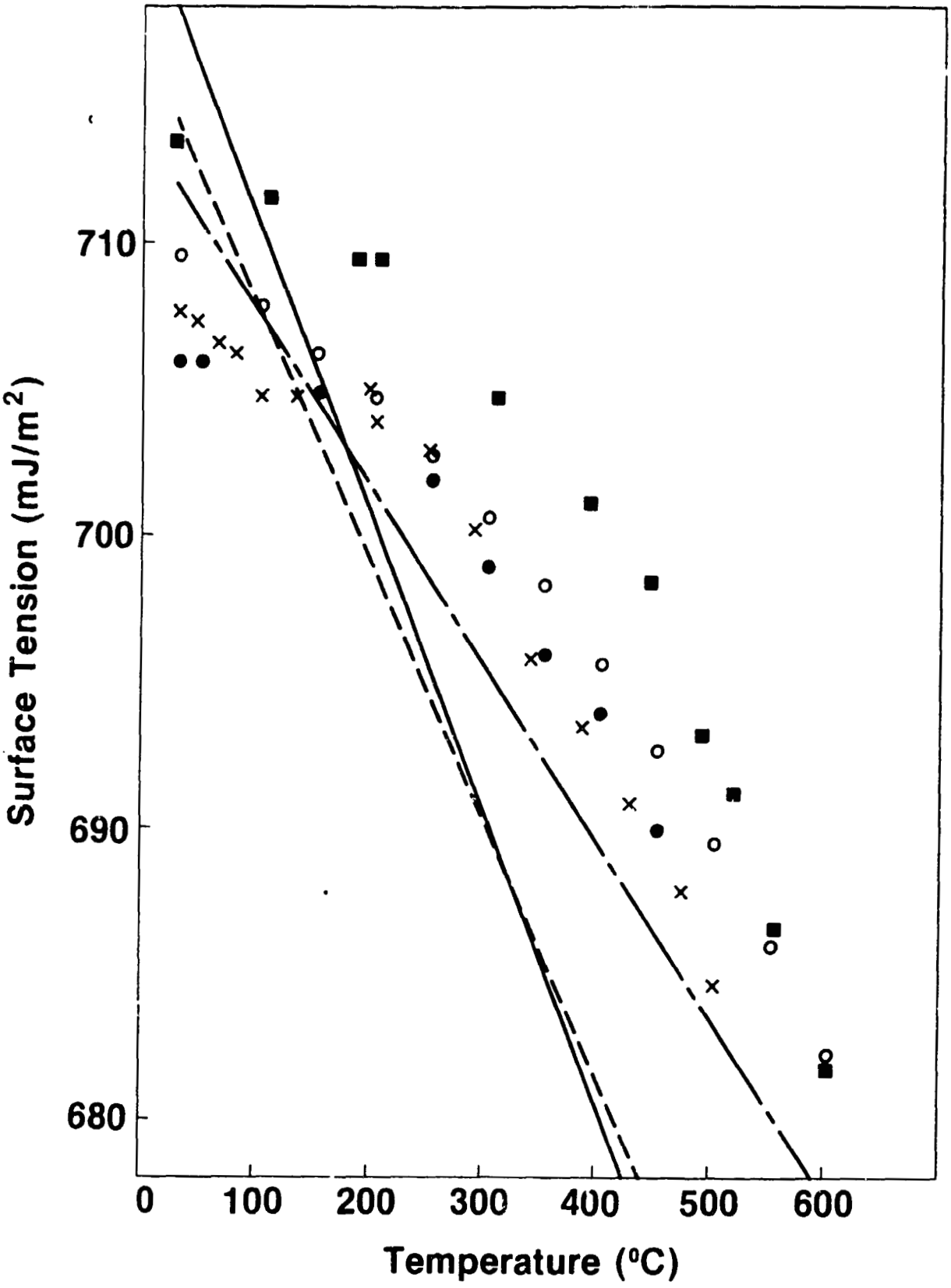

Figure 1. Summary of previous measurements of the surface tension of gallium: ref. (1) O; ref. (2) ●; ref. (3) X ; ref. (4) —; ref. (5)– –; ref. (6)—·—; Hardy (unpublished) ■ .

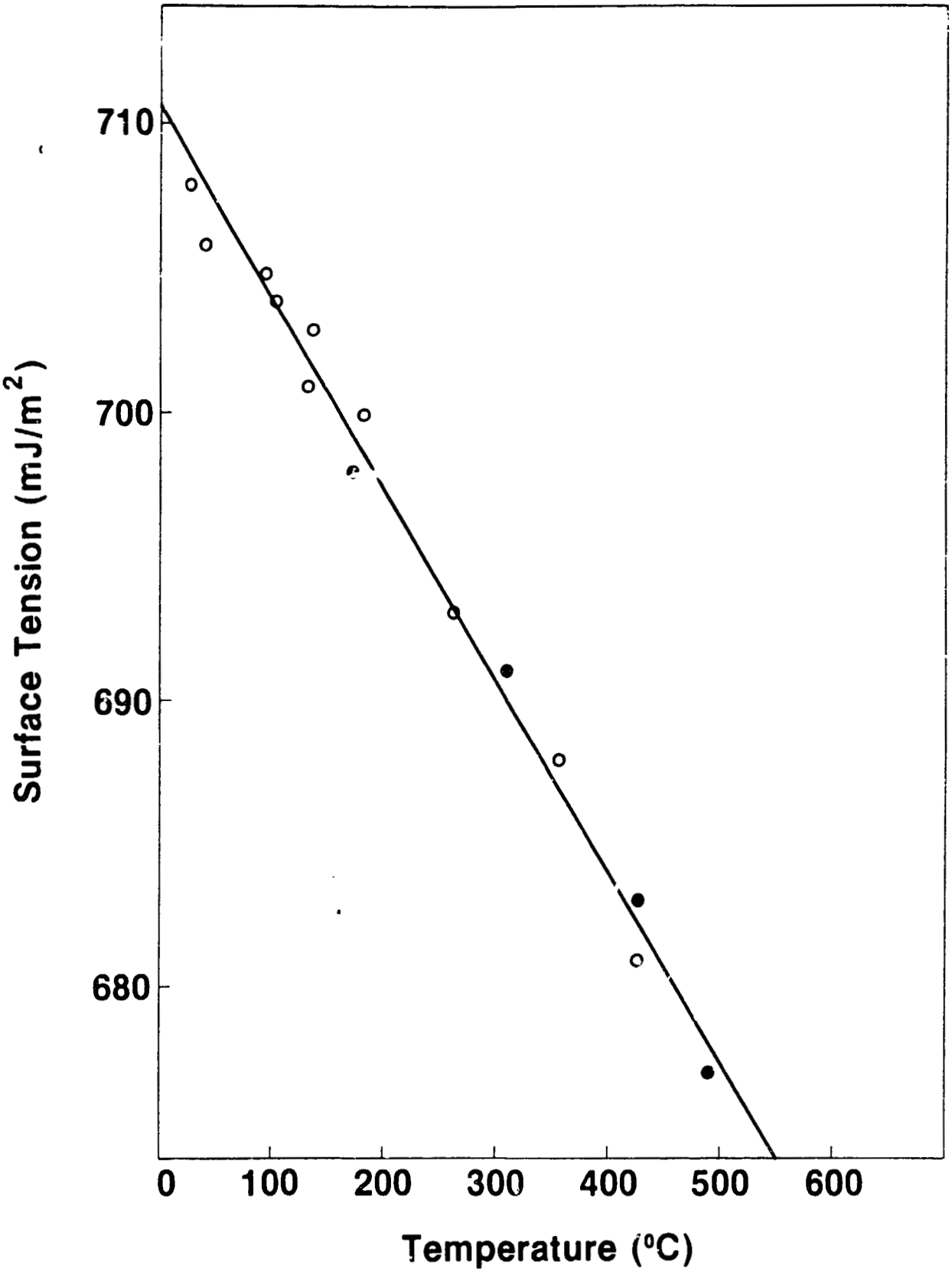

Figure 2. Surface tension of two gallium drops of different mass cleaned by argon ion sputtering.

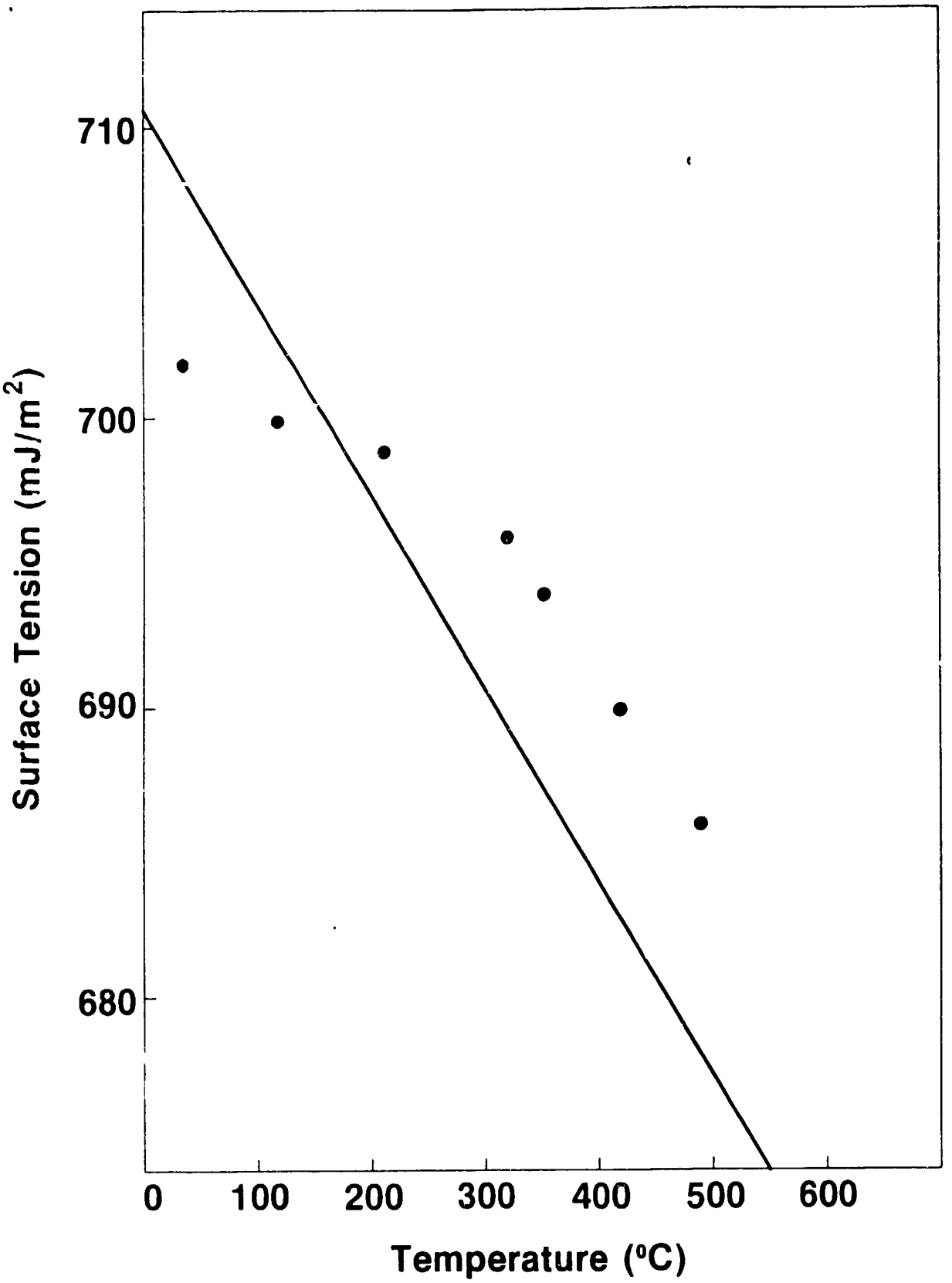

Figure 3. Measured surface tension of a gallium drop, a large fraction of whose surface is covered with solid impurity islands. The line (same as Figure 2) shows the behavior found when the islands are removed by sputtering.

Task 2

Convection during Unidirectional Solidification

S. R. Coriell, G. B. McFadden and R. J. Schaefer

Introduction

The general aim of this task is the theoretical and experimental study of the fluid flow, solute segregation, and interface morphology which occur during solidification. In particular, the role of thermosolutal convection (gravity driven flow due to temperature and solute gradients) during vertical directional solidification of a binary alloy is studied both theoretically and experimentally. A number of articles describing this research were published during the past year [1-8].

A brief review of work on this task and related research was presented at the Workshop on Microgravity Science and Applications, which was held at the Jet Propulsion Laboratory, Pasadena, CA on December 3-4, 1984; this review is reproduced in Appendix A. It appears that cellular growth experiments in the absence of fluid flow would provide definitive data and guidance in advancing current theories. Since the avoidance of fluid flow in earth-based directional solidification experiments appears extremely difficult, we are planning such experiments in collaboration with J. J. Favier and D. Camel of the Centre d'Etudes Nucleaires de Grenoble. In order to understand the differences between earth and space experiments, mathematical modelling of buoyancy driven convection for various geometries and for different gravitational levels (including time-dependent accelerations) will be continued.

We present a discussion of current numerical modelling first and then a description of the experimental work; each section can be read independently.

Numerical Results

Our previous calculations of thermosolutal convection during directional

solidification [6] assumed periodic boundary conditions on the vertical boundaries. This is a reasonable approximation when the horizontal wavelength is small compared to the lateral dimensions of the sample. When the wavelength is comparable to the lateral dimensions of the sample, it is clearly better to use boundary conditions appropriate for rigid walls and we have modified the numerical algorithm accordingly. The periodic boundary conditions correspond to $u = \partial v/\partial x = \partial T/\partial x = \partial c/\partial x = 0$ on the vertical boundaries; here u and v are the flow velocities in the x and y directions, respectively, T is the variation of the temperature from the temperature in the absence of flow, and c is the solute concentration (see reference 6 for a detailed description and notation). At a rigid wall the fluid velocity vanishes so that $u = v = 0$, and the solute flux vanishes so that $\partial c/\partial x = 0$. The boundary condition on the temperature variation depends on the thermal properties of the boundary, with two limiting possibilities being perfectly conducting ($T = 0$) or perfectly insulating ($\partial T/\partial x = 0$). We have assumed perfectly conducting boundaries, which implies that the temperature distribution on the boundary is independent of time. The rigid boundary conditions are then $u = v = T = (\partial c/\partial x) = 0$. We have also assumed perfectly conducting boundaries at the top and bottom of the sample so that $T = 0$ at these boundaries.

Numerical calculations were carried out for the following values of the dimensionless variables: $k_S/k_L = \kappa/\kappa_S = 1$, (thermal properties of crystal and melt are the same), Prandtl number Pr = 0.01, Schmidt number Sc = 10, distribution coefficient k = 0.3, crystal growth velocity U = 0.5, thermal Rayleigh number Ra = 1268, and aspect ratio (height/width) = 2. The Prandtl and Schmidt numbers are typical of semiconductor melts. Figures 1 and 2 show the steady state stream function and concentration fields for a solutal Rayleigh number Rs of 2000 for two different initial conditions. In Figure 1, the

flow is downward near both walls and upward in the middle, giving rise to a concentration profile which is symmetric about the midplane of the container. The dimensionless solute concentration in the crystal at the crystal-melt interface ranges from 0.88 at the wall to 1.24 at the center with an average value of 1.06. The deviation of the average value from unity is numerical inaccuracy due to the finite mesh size (16 intervals in the horizontal direction and 80 intervals in the vertical direction). In Figure 2, in the vicinity of the crystal-melt interface, the flow is downward near the left boundary and upward near the right boundary. The interface solute concentration increases from 0.73 at the left boundary to 1.84 at the right boundary. By symmetry, there is also a steady state solution in which the flow is the reverse of that of Figure 2, i.e., upward near the left boundary and downward near the right boundary. We did not find a steady state solution in which the flow is upward near the walls and downward in the middle.

For a system that is unbounded in the lateral direction, the critical solutal Rayleigh number for the onset of convection is 963 for the values of the dimensionless parameters previously given [6]. The linear stability of the system with rigid vertical walls was determined using the nonlinear code; the onset of convection occurred at a solutal Rayleigh number of about 400. Thus, the system with rigid walls is less stable than the laterally unbounded system. Since rigid walls should inhibit flow, the result was intriguing and we have investigated it further. A linear stability analysis for the directional solidification system with sidewalls is nontrivial since it can not be reduced to ordinary differential equations. Therefore, we have considered a model system with simple boundary conditions on the horizontal boundaries. A manuscript "Double-Diffusive Convection with Sidewalls" by G. B. McFadden, S. R. Coriell, and R. F. Boisvert, describes results obtained

from this model and is reproduced in Appendix B. When the boundary conditions on temperature and concentration are not identical, rigid walls can actually destabilize the system for certain values of the governing parameters. An area of further research is the development of a numerical algorithm for similar linear stability calculations for a directional solidification system.

A number of linear stability calculations for laterally unbounded directional solidification have been carried out in collaboration with various groups interested in particular alloys and growth conditions. The critical solute concentration for the onset of convective and morphological instabilities during the directional solidification of aluminum containing magnesium has been calculated for various gravitational accelerations and temperature gradients. Thermophysical properties for the Al-Mg alloy were provided by Stephan Rex and Professor Peter R. Sahm (of the Giesserei-Institut der RWTH Aachen), who are experimentally investigating these alloys. Recent research by Caroli et al [9] have suggested that the onset of convective instability may be oscillatory in time in the lead-tin system at very low temperature gradients in the liquid. We have carried out linear stability calculations at a crystal growth velocity of 10 μm/s and a temperature gradient in the liquid of 0.1 K/cm. The convective instability is oscillatory in time and the behavior is similar to that in the succinonitrile-ethanol system [5]. Under conditions for which growth vertically upwards is convectively or morphologically unstable, it is worthwhile to consider the possibility of growth vertically downward. In collaboration with J. J Favier of the Centre d'Etudes Nucleaires de Grenoble, a number of linear stability calculations for the growth vertically downward of lead containing tin have been carried out. The onset of instability is usually oscillatory in time. Further linear

stability and nonlinear calculations will be performed to elucidate the advantages and disadvantages of downward growth.

Experimental

Convective effects induced by the presence of a second fluid phase near the solid-liquid interface have been further investigated by the use of a succino itrile sample containing a droplet of mercury. This system was chosen on the basis of assumed negligible mutual solubility and a large difference in thermal conductivity. Because of its high conductivity relative to succinonitrile, the surface of the mercury drop was effectively isothermal even in the presence of large thermal gradients in the surrounding succinonitrile. As a result, the isotherms in the succinonitrile were severely distorted and bouyancy-driven convection was present in the succinonitrile. Convective flow was seen even when the mercury drop lay just below the succinonitrile solid-liquid interface, so that no fluid-fluid interface was present. Irreproducibility in the shape of the mercury drop made quantitative rate measurements meaningless, but the fluid flow in this case did not differ noticeably from that which was present when the mercury drop contacted the liquid succinonitrile, thus implying that Marangoni convection was not playing an important role.

Earlier experiments on the effect of a gas bubble at the solid-liquid interface of a succinonitrile-ethanol alloy had shown that a greatly increased fluid flow was present in the vicinity of the bubble following slight motions of the bubble. The effect was attributed to Marangoni convection induced by transient gradients resulting from the bubble motion. The effect was not observed in the case of the mercury drop sample, where there should be no thermal gradients and no composition gradients (due to the absence of the ethanol).

The experiments thus suggest that a second fluid phase can induce convection near the solid-liquid interface both by distortion of the thermal field and by the Marangoni effect. The first mechanism would of course be greatly reduced by microgravity, but the second mechanism would continue to operate. The importance of controlling the free volume generated by solidification shrinkage during space flight experiments is thus emphasized.

In cooperation with Centre d'Etudes Nucleaire de Grenoble (CENG) of Grenoble, France, we are studying methods for demarkation of solid-liquid interfaces during directional solidification of metals. These methods would be employed during flight experiments on the MEPHISTO apparatus to determine interface shapes at different temperature gradients and growth velocities.

The shape of the solid-liquid interface during solidification of semiconductor materials can be marked within the growing solid by Peltier pulsing. In this method, a pulse of electric current is passed through the sample, normal to the solid-liquid interface, with the result that Peltier heat is emitted or absorbed at the interface, depending on the direction of current flow. This Peltier pulse causes a transient change of the solidification rate, which causes a corresponding change in the composition of the solid. Upon subsequent metallographic examination, the shape of the interface at the time of the pulse is revealed by the compositional transient. The Peltier effect has the advantage that heat is absorbed or emitted directly at the solid-liquid interface, but unfortunately Peltier pulse marking of metallic solid-liquid interfaces is difficult because of the low Peltier coefficients of metal solid-liquid interfaces.

There are, however, other ways in which marking transients can be produced. One requirement is that the transient be brief enough that it not

cause a significant change in the interface shape. For this reason we are initiating a series of experiments in which the interface will be perturbed by very short pulses of electric current. Such pulses can be made very large, in which case the effect of Joule heating will be greater than that of Peltier heating or cooling. The effectiveness of the pulses will be measured as a function of several variables to obtain the best marking with the minimum disturbance of the interface.

References

1. Coupled Convective Instabilities at Crystal-Melt Interfaces, S. R. Coriell, G. B. McFadden, R. F. Boisvert, M. E. Glicksman, and Q. T. Fang, J. Crystal Growth 66 (1984) 514-24.

2. Asymmetric Instabilities in Buoyancy-Driven Flow in a Tall Vertical Annulus, G. B. McFadden, S. R. Coriell, R. F. Boisvert, and M. E. Glicksman, Phys. Fluids 27 (1984) 1359-61.

3. The Effect of Anisotropic Crystal-Melt Surface Tension on Grain Boundary Groove Morphology, P. W. Voorhees, S. R. Coriell, G. B. McFadden and R. F. Sekerka, J. Crystal Growth 67 (1984) 425-40.

4. Effect of a Forced Couette Flow on Coupled Convective and Morphological Instabilities During Unidirectional Solidification, S. R. Coriell, G. B. McFadden, R. F. Boisvert, and R. F. Sekerka, J. Crystal Growth 69 (1984) 15-22.

5. Convection-Induced Distortion of a Solid-Liquid Interface, R. J. Schaefer and S. R. Coriell, Met. Trans. 15A (1984) 2109-15.

6. Thermosolutal Convection during Directional Solidification, G. B. McFadden, R. G. Rehm, S. R. Coriell, W. Chuck, and K. A. Morrish, Met. Trans. 15A (1984) 2125-37.

7. Morphological Stability in the Presence of Fluid Flow in the Melt, G. B. McFadden, S. R. Coriell, R. F. Boisvert, M. E. Glicksman, and Q. T. Fang, Met. Trans. 15A (1984) 2117-24.

8. Convective Influence on the Stability of a Cylindrical Solid-Liquid Interface, Q. T. Fang, M. E. Glicksman, S. R. Coriell, G. B. McFadden, and R. F. Boisvert, J. Fluid Mech. 151 (1985) 212-40.

9. Solutal Convection and Morphological Instability in Directional Solidification of Binary Alloys, B. Caroli, C. Caroli, C. Misbah, and B. Roulet, J. Phys. Paris 46 (1985) 401-13.

Figure 1

RS = .20000 + 004 RA = .12680 + 004 SC = 10.000 P = .0100 LV/D = 5.000

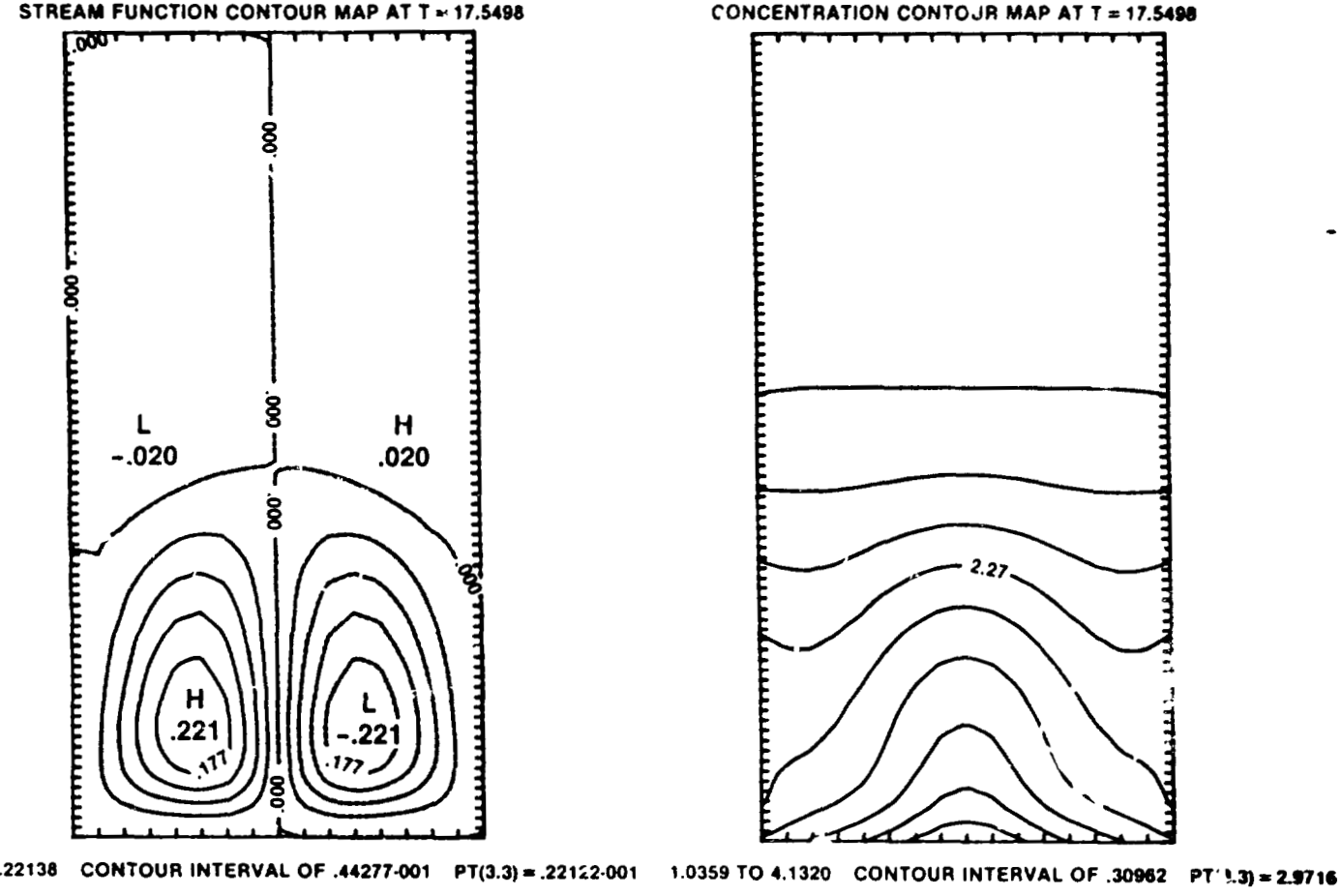

-.22138 TO .22138 CONTOUR INTERVAL OF .44277-001 PT(3.3) = .22122-001 1.0359 TO 4.1320 CONTOUR INTERVAL OF .30962 PT(3.3) = 2.9716

Figure 2

RS = .20000 + 004 RA = .12680 + 004 SC = 10.000 P = .0100 LV/D = 5.000

STREAM FUNCTION CONTOUR MAP AT T = 18.4078

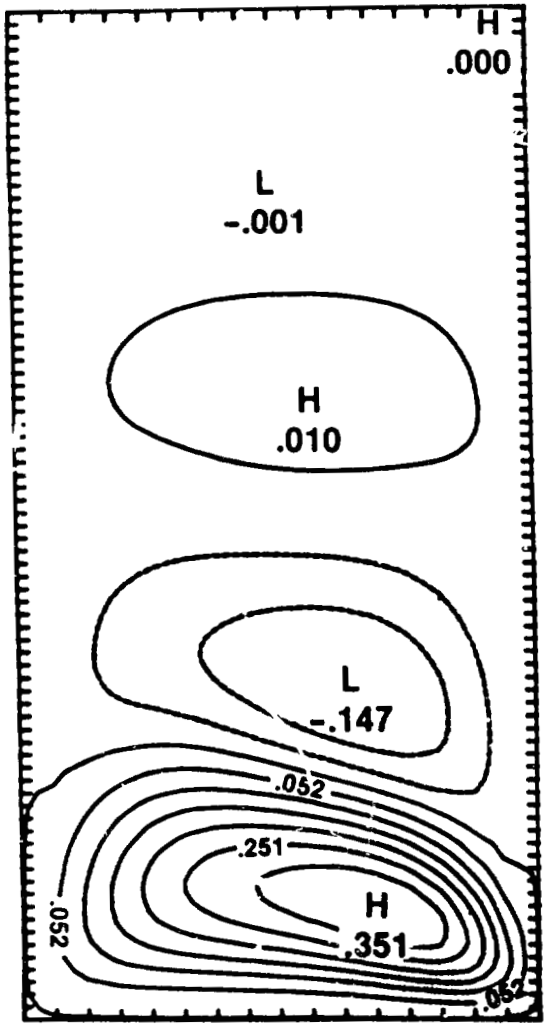

-.14664 TO .35080 CONTOUR INTERVAL OF .49724-001 PT(3.3) = .26802-001

CONCENTRATION CONTOUR MAP AT T = 18.4078

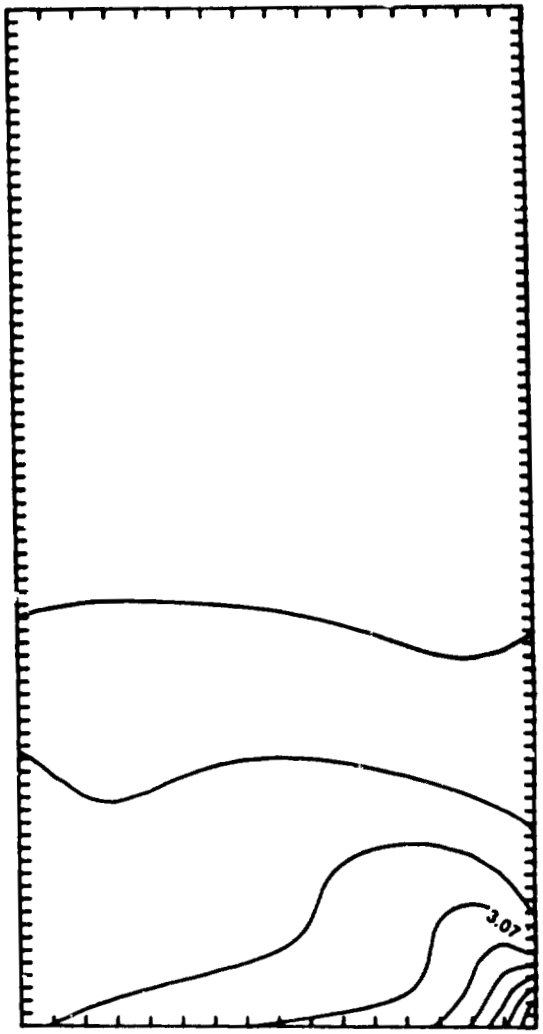

1.0260 TO 6.1415 CONTOUR INTERVAL OF .51155

APPENDIX A

Proceedings of Workshop on Microgravity Science and Applications
Pasadena, CA; December 3-4, 1984

Convection and Interface Stability during Solidification

S. R. Coriell

During a first order phase transformation, the motion of the interface between the two phases depends on the transport of heat and solute. For alloy solidification or crystal growth from the melt, the parent phase is a fluid and the transport is by both diffusion and convection. For metallic alloys, thermal diffusivities, κ, are four orders of magnitude greater than solute diffusivities, D, so that fluid flow has a much greater effect on solute distribution than on the temperature field. The solute distribution at the crystal-melt interface directly determines the solute distribution in the solidified material since diffusion rates in the solid are generally extremely small.

The general problem of mathematical modelling of fluid flow during solidification is challenging since it involves the non-linear Navier-Stokes equations and a Stefan problem, i.e., the boundary conditions on the temperature, concentration, and fluid flow fields are specified at the solid-liquid interface whose position is unknown. The temperature, concentration, and fluid flow fields are not only coupled through the convective and buoyancy terms in the field equations but also through the boundary conditions at the solid-liquid interface. These boundary conditions directly couple the temperature and solute field since the melting point depends on composition, and indirectly couple the fluid flow field to the temperature and concentration field, since the position of the interface is determined by these fields. Further, the role played by the solid-liquid surface energy requires calculation of the mean curvature of the solid-liquid interface. For metals and semiconductors, the Prandtl number ($Pr = \nu/\kappa$ where ν is the kinematic viscosity)

is of the order of 10^{-2} and the Schmidt number ($Sc = \nu/D$) is the the order of 10^2; these parameters indicate widely different length and time scales for mass, momentum, and energy transport and may cause additional numerical problems.

Directional solidification of a binary melt to form a single phase solid at constant velocity V is most amenable to theoretical analysis and is a good approximation to directional solidification experiments in which there is uniform relative motion of the sample and its thermal environment. Since the solute concentration of a liquid is usually quite different from that of a solid with which it is in equilibrium, there is either rejection or preferential incorporation of solute by the solid at a moving crystal-melt interface. This results, for a quiescent liquid, in an exponential concentration gradient that extends ahead of the interface with a characteristic distance of D/V. The temperature gradient is also exponential with characteristic distance κ/V; however, κ/V is usually sufficiently large that the temperature gradient is essentially constant within each phase.

If the crystal-melt interface is planar and there is no fluid flow in the melt, then at steady state the solidified material will have a uniform solute distribution. Even in the absence of convection, it is well known that for sufficiently high solute concentrations the crystal-melt interface will be unstable [1], and develop into a cellular or dendritic interface with lateral solute segregation (microsegregation). For small solidification velocities (typically less than 10^{-2} cm/s), an excellent approximation to the stability criterion is the modified constitutional supercooling criterion, i.e., the planar interface is stable if

$$G^*/(mG_c) > 1$$

with

$$G^* = (k_S G_S + k_L G_L)/(k_S + k_L)$$

where k_L and k_S are thermal conductivities of liquid and solid, respectively, G_L and G_S are unperturbed temperature gradients at the interface in the liquid and solid, respectively, m is the change in melting temperature with solute concentration, and G_C is the unperturbed solute gradient at the interface in the liquid. The product mG_C is always positive, even though solutes can either raise or lower the melting temperature. Basically, positive temperature gradients are stabilizing while the solute gradient is destabilizing. Another stabilizing influence, not evident in the equations, is the solid-liquid surface free energy, γ, which tends to minimize interfacial area. At small velocities, the surface energy has a negligible effect on the stability criterion but plays an important role in determining the wavelength λ at the onset of instability; typically these wavelengths are in the range 1-100 μm and decrease with increasing velocity.

Recently, there has been renewed theoretical interest in the nonlinear aspects of the morphologies that occur during directional solidification. For interface shapes that do not differ too much from planarity, the free boundary problem may be handled by means of linear stability analysis [1] and non-linear expansion techniques [2]. High speed computers have made possible numerical calculations of nonplanar interface morphologies that differ significantly from planarity [3-4]. Since cellular spacings are generally orders of magnitude smaller than sample dimensions, computational domains with periodic boundary conditions corresponding to wavelengths of anticipated cell spacings are used. In general, it is possible to find a family of steady state solutions (interface shapes, temperature and concentration fields) for

a range of wavelengths. The fundamental problem of wavelength selection has been longstanding and is just beginning to be understood [5].

Steady state two-dimensional interface shapes and interface concentrations are shown in Figure 1. The three calculations [4] correspond to bulk alloy concentrations that exceed the critical concentration for instability by 0.5, 4.0, and 13.0 percent. The cell groove deepens and accompanying solute segregation increases rapidly as the bulk concentration is raised. Recent work by Ungar and Brown [6] successfully follows the evolution of cells to groove depths of up to fifteen times their wavelength. A nonlinear stability analysis of three-dimensional cells has recently been carried out by Sriranganathan et al. [2] in an attempt to understand the complex morphologies which have been observed experimentally. For example in lead-antimony alloys [7], the interface morphology at the onset of instability depended on crystallographic orientation; nodes (circular wells of liquid penetrating into the crystal) developed when the growth direction was near [100] or [111] while elongated cells developed near [110]. At higher degrees of instability, regular (hexagonal) cells developed.

It is well known that horizontal temperature and concentration gradients give rise to buoyancy driven fluid flow [8]. In order to minimize these horizontal gradients growth should be in the vertical direction. For a normal liquid, which expands on heating, growth vertically upwards will ensure that in the absence of solute the liquid density will decrease with height. However, even for this growth configuration since container walls are not perfectly adiabatic, the differences in thermal conductivity between crystal, melt, and container, and the latent heat released on freezing will give rise to horizontal temperature gradients, resulting in fluid flow. The nature of this flow in

prototype crystal growth systems is beginning to be understood through extensive numerical modelling [9]. For vertical growth in the absence of horizontal temperature and concentration gradients, a motionless solution will formally satisfy the fluid flow equations; however, such a solution is not necessarily stable and convective instability may occur.

When both the temperature and solute fields individually cause the density to decrease with height, there is no possibility of convective instability. However, even in this case, there can be undesirable convective effects. During measurements of cell spacings in Al-6 wt% Cu alloys, McCartney and Hunt [10] observed that the macroscopic interface was highly curved. Since the curvature could be eliminated by using the ternary system Al-Mg-Si, which has a very low value of the temperature derivative of the liquid density along the liquidus line, convection appears important in the stably stratified Al-Cu system. Presumably, convection due to horizontal temperature gradients interacts with the solute gradient to cause a non-uniform solute concentration at the interface.

If a solute that is rejected at the crystal-melt interface decreases the density of the melt or a solute that is preferentially incorporated at the crystal-melt interface increases the density of the melt, then the solute field in the absence of a temperature gradient will cause the liquid density to increase with height during growth vertically upwards, and there is the possibility of convective instability. The unperturbed static density profile due to both temperature and concentration variation is of little utility in predicting the onset of convection since one can have a statically unstable density profile without convection and a statically stable density profile with convection. The latter case of convection, even though the liquid density

decreases with height, is a feature of double diffusive convection and arises due to the difference in diffusivities of the two diffusing species, viz., solute and heat [11]. The results of linear stability analysis [12] of combined morphological and double diffusive convective instabilities is shown in Figure 2 for the growth vertically upwards of lead containing tin with a temperature gradient in the liquid of 200 K/cm for three different constant gravitational accelerations. The system is unstable for tin concentrations c_∞ above the curves. The upper line with negative slope represents the onset of morphological instability, and is essentially independent of the gravitational acceleration. The three curves labelled with values of the gravitational acceleration represent the onset of convective instability, and are very sensitive to the gravitational acceleration. For tin concentrations below the dashed-dot curve the static liquid density decreases with height. Extremely small amounts of solute can cause convective instability in experiments on Earth, e.g., at a growth velocity of 1 μm/s the critical tin concentration is $3.2(10^{-4})$ wt%. Additional calculations for a growth velocity of 1 μm/s show that a vertical magnetic field of 1 tesla increases the critical concentration by an order of magnitude.

The behavior of the convective stability curves shown in Figure 2 can be qualitatively understood by recognizing that the relevant length scale is the diffusion distance D/V. The thermal Rayleigh number Ra is then proportional to $G_L(D/V)^4$ and the solutal Rayleigh number is proportional to $G_c(D/V)^4$ or equivalently $c_\infty(D/V)^3$. For fixed G_L and large growth velocities the thermal Rayleigh number becomes very small and stability is determined by a balance of the destabilizing solute field and the stabilizing viscous forces; instability occurs when the solutal Rayleigh number exceeds about ten [13].

For small growth velocities the thermal Rayleigh number is large, and stability is determined by a balance of the destabilizing solute field and the stabilizing thermal field; the solutal and thermal Rayleigh numbers are roughly comparable.

The coupling between morphological and convective modes of instability is rather weak except near the concentrations and velocities at which the morphological and convective curves cross in Figure 2. In the vicinity of this crossing instabilities which are oscillatory in time may occur.

In order to determine the extent of solute segregation and the nature of flow field caused by double diffusive convection during directional solidification, the time dependent nonlinear differential equations for fluid flow, concentration, and temperature have been solved numerically in two spatial dimensions for small Prandtl numbers and large Schmidt numbers [14]. For slow solidification velocities, the thermal field has an important stabilizing influence: near the onset of instability the flow is confined to the vicinity of the crystal-melt interface. Further, for slow velocities, as the concentration increases, the horizontal wavelength of the flow decreases rapidly--a phenomenon also indicated by linear stability analysis. For a narrow range of solutal Rayleigh numbers and wavelengths, the flow is periodic in time.

The steady state stream function and solute field as a function of position for a semiconductor melt (Schmidt number of 10 and Prandtl number of 0.01) is shown in Figure 3. The crystal-melt interface, assumed planar in the calculations, is located at the bottom of the figures, and the interface concentration varies by about 60 percent along the interface. For this calculation, the thermal Rayleigh number is large and the solutal Rayleigh number exceeds the critical solutal Rayleigh number for the onset of convection by only 30 percent so that the flow is confined to the vicinity of the crystal-

melt interface. The maximum flow velocities are relatively small. For example, for a lead-tin alloy at a growth velocity of 2.0 μm/s and a liquid temperature gradient of 200 K/cm, the maximum flow velocity was 17.0 μm/s when the bulk concentration exceeded the critical concentration for instability by a factor of 4.3. However, this flow velocity is sufficient to cause a 30 percent variation in the solute concentration at the crystal-melt interface.

We discuss briefly a few experiments which demonstrate the effects of convection during directional solidification. Boettinger et al [15] studied the growth of lead rich lead-tin off-eutectic alloys. For growth vertically upwards, the solute field is destabilizing and substantial variation in composition in the growth direction (macrosegregation) was found. A vertical or horizontal magnetic field of 0.1 Tesla did not reduce the macrosegregation, but downward solidification in small (3 mm) diameter tubes virtually eliminated the macrosegregation. Sample and Hellawell [16] have recently investigated the mechanisms of channel segregation during alloy solidification vertically upwards. Channels containing high solute concentrations develop from positions near a dendritic growth front when the solute is less dense than the melt, and plumes rise to the top of the bulk liquid. Recent experiments by Schaefer [17] on the directional solidification vertically upward of succinonitrile containing ethanol have shown an interesting interaction between thermal convection due to radial temperature gradients and the solute field. For growth conditions near the onset of morphological instability, a macroscopic pit develops in an otherwise slightly curved crystal-melt interface. The flow is basically down near the container walls and upward near the axis of the tube. The solute concentration is increased near where the flow turns upward, and the macroscopic pit occurs in this region. Morphological instability

then takes place in the pit, and the pit disappears leaving a region of cellular growth in its place.

Except for a very limited range of parameters, the double diffusive and morphological instabilities which occur during directional solidification are rather weakly coupled. In particular, the short wavelength morphological mode is essentially unaffected by the possibility of convection in the quiescent liquid. Due to very different length scales for convective motions and for cellular interfaces, it will be extremely challenging to model the effect of convection on cellular morphologies. Various simplified models for the effect of a fully developed flow on morphological instability have been recently reviewed [18]. Delves [19] has calculated the effect of forced flow parallel to the crystal-melt interface on the onset of morphological instability. The effect of such a flow on combined double diffusive and morphological instabilities has recently been treated for Couette flow [20]. Such a flow does not affect perturbations with wave vectors perpendicular to the flow. For perturbations with wave vectors parallel to the flow, the onset of morphological instability is somewhat suppressed and double diffusive instability is greatly suppressed. When instabilities occur, they are oscillatory and correspond to travelling waves. A complicated flow field could be approximated in the vicinity of the crystal-melt interface by a simple flow such as a Couette flow. This would simplify the modelling of the interaction between fluid flow and the crystal-melt interface. However, Glicksman and colleagues [21-23] have recently demonstrated a coupling between hydrodynamic and morphological instabilities for which such an approximation is clearly incorrect.

We conclude with a brief description of this coupled instability. A

long vertical cylindrical sample of high purity succinonitrile was heated by an electrical current passed through a long coaxial heating wire, so that a vertical melt annulus formed between the coaxial heating wire and the surrounding crystal-melt interface. The outer radius of the crystal was maintained at a constant temperature below the melting point of the material. This arrangement permits the temperature to decrease monotonically from the melt to the solid across the crystal-melt interface, and consequently the interface would be morphologically stable in the absence of fluid flow.

The thermal gradients in the melt induce buoyancy forces which cause the fluid to flow upward near the heating wire on the axis and downward near the crystal-melt interface. When linear stability analysis is used to calculate the critical Grashof number for instabilities of the axisymmetric flow occurring between two vertical infinite rigid coaxial cylinders held at different temperatures, it is found that for a Prandtl number of 23 (corresponding to succinonitrile), the flow is unstable to an axisymmetric perturbation above a Grashof number of the order of 2000, and the resulting wave speed of this perturbation is comparable to the maximum in the characteristic unperturbed flow velocity.

In contrast, the experimental observations with a crystal-melt interface indicate an asymmetric helical instability at a critical Grashof number of about 150 with a wave speed two orders of magnitude less than the unperturbed flow velocity. Linear stability analysis reveals that the instability is due to a coupling between a basic hydrodynamic instability in the buoyant flow and the deformable crystal-melt interface. The crystal-melt interface lowers the critical Grashof number of an analogous rigid-walled system by an order of magnitude; furthermore, the hydrodynamic mode that is actually destabilized by the interface is not the least stable mode in the rigid-walled system. The

calculations show that the instability may be regarded either as a large alteration of a basic hydrodynamic instability by the crystal-melt interface, or as a significant modification of the morphological stability of the interface by the presence of the buoyant flow. The instability is sensitive to the form of the flow field; e.g., it does not occur for Couette or Poiseuille flows.

References

1. W. W. Mullins and R. F. Sekerka, Stability of a Planar Interface During Solidification of a Dilute Binary Alloy, J. Appl. Phys. 35, 444 (1964).

2. R. Sriranganathan, D. J. Wollkind, and D. B. Oulton, A Theoretical Investigation of the Development of Interfacial Cells During the Solidification of a Dilute Binary Alloy: Comparison with the Experiments of Morris and Winegard, J. Crystal Growth 62, 265 (1983).

3. L. H. Ungar and R. A. Brown, Cellular Interface Morphologies in Directional Solidification. The One-Sided Model, Phy. Rev. B29, 1367 (1984).

4. G. B. McFadden and S. R. Coriell, Nonplanar Interface Morphologies During Unid rectional Solidification of a Binary Alloy, Physica 12D, 253 (1984).

5. J. S. Langer, Pattern Selection in Solidification, Met. Trans. 15A, 961 (1984).

6. L. H. Ungar, Directional Solidification from a Bifurcation Viewpoint, Ph. D. thesis 1984, MIT, Cambridge, MA.

7. L. R. Morris and W. C. Winegard, The Development of Cells During the Solidification of a Dilute Pb-Sb Alloy, J. Crystal Growth 5, 361 (1969).

8. D. D. Joseph, Stability of Fluid Motions II (Springer, Berlin, 1976).

9. C. J. Chang and R. A. Brown, Radial Segregation Induced by Natural Convection and Melt/Solid Interface Shape in Vertical Bridgman Growth, J. Crystal Growth 63, 343 (1983).

10. D. G. McCartney and J. D. Hunt,Measurements of Cell and Primary Dendrite Arm Spacings in Directionally Solidified Aluminium Alloys, Acta Met. 29, 1851 (1981).

11. J. S. Turner, Buoyancy Effects in Fluids (Cambridge Univ., Cambridge, 1973).

12. S. R. Coriell, M. R. Cordes, W. J. Boettinger, and R. F. Sekerka, Convective and Interfacial Instabilities During Unidirectional Solidification of a Binary Alloy, J. Crystal Growth 49, 13 (1980).

13. D. T. J. Hurle, E. Jakeman, and A. A. Wheeler, Hydrodynamic Stability of the Melt During Solidification of a Binary Alloy, Phys. Fluids 26, 624 (1983).

14. G. B. McFadden, R. G. Rehm, S. R. Coriell, W. Chuck, and K. A. Morrish, Thermosolutal Convection During Directional Solidification, Met. Trans. 15A, 2125 (1984).

15. W. J. Boettinger, F. S. Biancaniello, and S. R. Coriell, Solutal Convection Induced Macrosegregation and the Dendrite to Composite Transition in Off-Eutectic Alloys, Met. Trans. 12A, 321 (1981).

16. A. K. Sample and A. Hellawell, The Mechanism of Formation and Elimination of Channel Segregation During Alloy Solidification, Met. Trans. 15A, 2163 (1984).

17. R. J. Schaefer and S. R. Coriell, Convection-Induced Distortion of a Solid-Liquid Interface, Met. Trans. 15A, 2109 (1984).

18. S. R. Coriell and R. F. Sekerka, Effect of Convective Flow on Morphological Stability, PhysicoChemical Hydrodynamics 2, 281 (1981).

19. R. T. Delves, Theory of Interface Stability, in Crystal Growth, ed. B. R. Pamplin (Pergamon, Oxford, 1974).

20. S. R. Coriell, G. B. McFadden, R. F. Boisvert, and R. F. Sekerka, Effect of a Forced Couette Flow on Coupled Convective and Morphological Instabilities During Unidirectional Solidification, J. Crystal Growth 69, 15 (1984).

21. Q. T. Fang, M. E. Glicksman, S. R. Coriell, G. B. McFadden, and R. F. Boisvert, Convection Influence on the Stability of a Cylindrical Solid-Liquid Interface, J. Fluid Mech. 151, 212 (1984).

22. G. B. McFadden, S. R. Coriell, R. F. Boisvert, M. E. Glicksman, and Q. T. Fang, Morphological Stability in the Presence of Fluid Flow in the Melt, Met. Trans. 15A, 2117 (1984).

23. S. R. Coriell, G. B. McFadden, R. F. Boisvert, M. E. Glicksman, and Q. T. Fang, Coupled Convective Instabilities at Crystal-Melt Intefaces, J. Crystal Growth 56, 514 (1984).

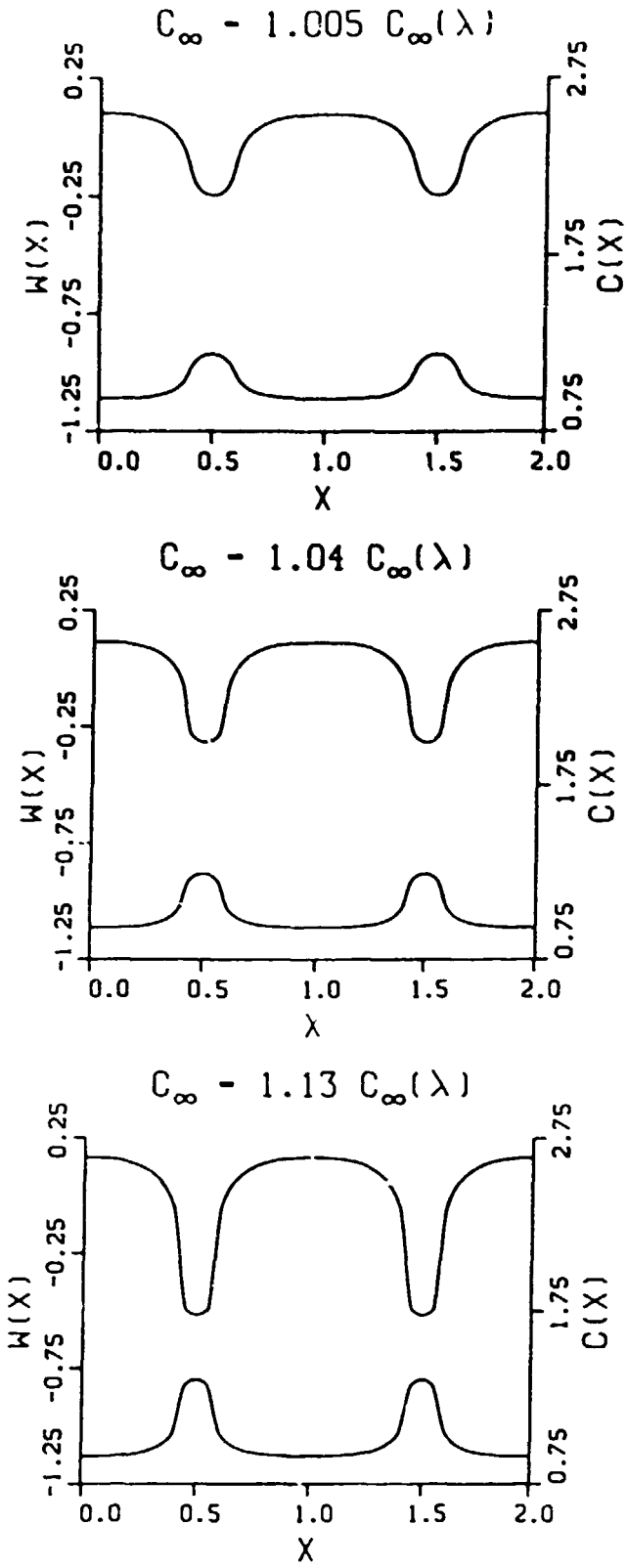

Fig. 1. Plots of interface shape and distribution of solute in the solid for a given wavelength as the bulk concentration is increased. The top curve in each plot is the interface shape, the bottom curve is the concentration of solute. Two wavelengths are shown.

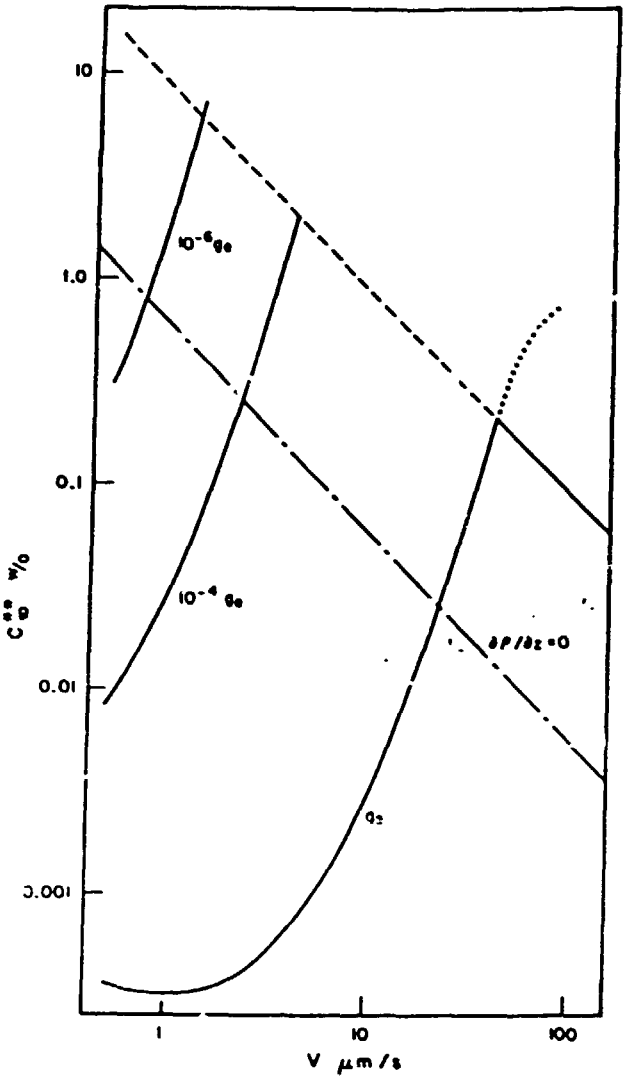

Figure 2. The critical concentration c_∞^{**} of tin in lead above which instability occurs as a function of the velocity V of directional solidification for a temperature gradient G_L in the liquid of 200 K/cm. The solid curves represent gravitational accelerations g_e = 980 cm/s^2, 10^{-4} g_e, and 10^{-6} g_e. The upper line with negative slope represents the onset of morphological instabilities; the nearly parallel dashed-dot line labeled $(\partial\rho/\partial z) = 0$ represents the neutral density criterion. The dotted extension of the curve labeled g_e corresponds to oscillatory instabilities.

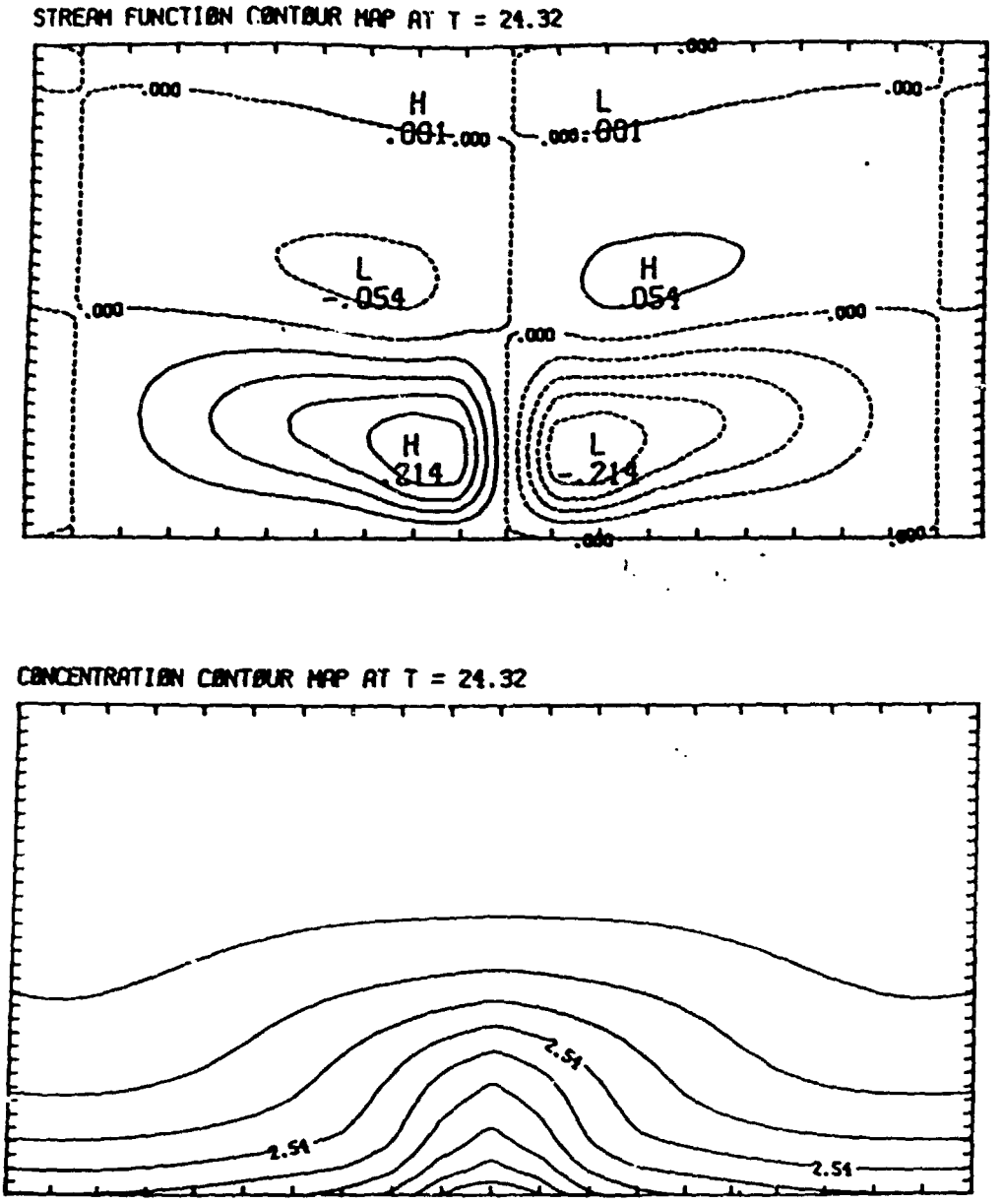

Figure 3.
The steady state stream function and concentration as a function of position for a bulk concentration 29% above the critical concentration for the onset of convection. Parameters used in the calculation are typical of semiconductor melts. In the concentration plot, the increment of (dimensionless) concentration between contours is 0.37. The maximum flow velocity is about 5 times the crystal growth velocity of typically 20 μm/s.

On Double-Diffusive Convection with Sidewalls

G. B. McFadden, S. R. Coriell, and R. F. Boisvert
National Bureau of Standards
Gaithersburg, MD 20899

Abstract

The effect of rigid vertical boundaries on the onset of convective instability is calculated for the salt finger regime of double diffusive convection. The unperturbed state is a quiescient fluid with constant vertical gradients of temperature and solute, which are stabilizing and destabilizing, respectively. The horizontal boundaries are taken to be stress-free and perfectly conducting. The lateral boundaries are perfectly insulating for solute. Changing from thermally insulating to thermally conducting sidewalls results in a strong destabilization of the flow for large thermal Rayleigh numbers even in the limit that the separation between the sidewalls approaches infinity. Further, for thermally conducting sidewalls, a decrease in the separation of the sidewalls may destabilize the system.

47.20

1. Introduction

For a fluid in a gravitational field with two diffusing components present, for example, temperature and solute, it is well known that convective instabilities may occur even though the fluid density is strictly decreasing with height. This instability, known variously as thermosolutal convection, thermohaline convection, or double-diffusive convection, was first described by Stommel et al in 1956 [1] and has since been reviewed extensively [2-4]. This instability is of practical importance in many diverse areas involving convection and heat transfer; see e.g. [5]. In what follows, the instability will be described in terms of the diffusion of heat and salt in a differentially heated saline solution. The density of a fluid parcel then depends on its temperature and salinity: heating the parcel makes it lighter and salting it makes it heavier. Of primary importance is the feature that the diffusion of heat occurs much more rapidly than does the diffusion of solute.

Consider a vertical density stratification (uniform in the horizontal directions) with temperature and solute profiles that have opposite effects on the vertical density profile; that is, when considered separately, one would tend to increase, and the other decrease, the density as a function of height. Two distinct regimes occur, depending on which of the two quantities is "unstably stratified." A fluid that is heated and salted from above (solute field unstably stratified) is in the "fingering" regime. The conventional heuristic description of the instability is as follows [3]. The upward displacement of a fluid parcel carries it to a region of hotter and saltier water. The temperature in the parcel is relatively quick to equilibrate with its surroundings, whereas the solute is significantly less quick to do so. The parcel then finds itself at about the same temperature, but with less

solute, than its neighbors, and so the upward displacement is reinforced by buoyancy. In the simplest model [2], the instability occurs with a monotonic time dependence ("exchange of stability").

A fluid heated and salted from below falls within the "diffusive" regime. In this case, as described by Stern [6], when a fluid parcel is displaced vertically, the relative lag in diffusion rates may result in an overcompensating restoring force that causes "overstability" to develop, leading to a time-dependent, oscillatory behavior.

The present paper is concerned with the effect of sidewalls on flow in the fingering regime in the absence of applied horizontal gradients. The work was motivated by numerical results obtained from a simulation of thermosolutal convection occurring during the unidirectional solidification of a binary alloy. In this case, the unperturbed solute field in the liquid ahead of the solidifying planar interface has an exponential vertical profile due to the rejection or preferential incorporation of solute by the solid phase. The linear stability of the unperturbed problem for a system that extends to infinity in the horizontal directions is then non-trivial due to the vertical variation of the unperturbed state, and results are obtained numerically [7]. Finite difference methods were subsequently employed to describe the evolution of the instabilities to finite amplitude [8]. In these calculations the two-dimensional flow was computed in a horizontally-periodic domain, consistent with the linear stability results for an infinite domain. When the lateral boundary conditions were altered to model the case of a finite container with rigid, perfectly conducting sidewalls that are perfectly insulating to solute, the instability was observed to set in at significantly lower Rayleigh numbers than for the infinite system. This result was unexpected; it was anticipated

that the addition of sidewalls would stabilize the flow as it does in the simpler case of a single-component system.

The linear stability for the directional solidification system with lateral sidewalls is intractable. For this reason an easier problem is considered here, consisting of a two-dimensional rectangular box with rigid, solutally insulating lateral walls, with constant vertical gradients of temperature and solute. We will mainly consider the sidewalls to be perfectly conducting for temperature; however we will contrast these results with previous results for perfectly insulating sidewalls, and will give a few results for mixed boundary conditions. As was observed by Drazin [9] for the single-component case, if the horizontal boundaries are taken to be stress-free and perfectly conducting, the solution is separable and the vertical dependence is simple. The linear stability is then governed by a set of constant-coefficient ordinary differential equations in the horizontal variable, so that the effect of the lateral boundary conditions on the stability of the base state can be examined in detail. We found that the addition of the sidewalls to the infinite system may result in a significant destabilization for a range of parametric values.

In section 2 we describe the governing equations for the system. In section 3 we describe briefly a fully numerical solution to the ordinary differential equations. In section 4 we give an independent check of the numerical results by finding zeroes of the characteristic determinant, which in this case may be expressed in terms of closed-form linearly-independent solutions to the governing equations. Results are presented in section 5, with a concluding discussion in section 6.

2. The Governing Equations

We consider a two-dimensional box of height H and width 2W. The sidewalls of the box are taken to be rigid, perfectly thermally conducting, and perfectly insulating to solute. Following Drazin [9], the top and bottom boundaries are taken to be stress-free and perfectly conducting to heat and solute. The fluid occupying the box is described by the Oberbeck-Boussinesq approximation to the Navier-Stokes equations [3]. The fluid is heated and salted from above, with values of the temperature and salt concentration (T_0', S_0') on the bottom boundary and $(T_0' + \Delta T, S_0' + \Delta S)$ on the top boundary with ΔT and ΔS positive. The density ρ' of the fluid is assumed to depend on the temperature T' and the salt concentration S' as

$$\rho' = \rho_0'(1 - \alpha[T' - T_0'] + \beta[S' - S_0'])$$

where α and β are both taken to be positive constants. The constant ρ_0' is the density at temperature T_0' and salinity S_0'.

In the Oberbeck-Boussinesq approximation the dimensionless governing equations take the form

$$-D(\nabla^2\psi)/Dt = -\nabla^2(\nabla^2\psi) + (Ra/Pr)(\partial T/\partial x) - (Rs/Sc)(\partial S/\partial x) \qquad (1)$$

$$DT/Dt = \nabla^2 T/Pr \qquad (2)$$

$$DS/Dt = \nabla^2 S/Sc \qquad (3)$$

for $-L < x < L$, $0 < y < 1$, where $L = W/H$, $D/Dt = \partial/\partial t + u\partial/\partial x + v\partial/\partial y$, $u = \partial\psi/\partial y$, $v = -\partial\psi/\partial x$, $T = (T' - T_0')/\Delta T$, $S=(S' - S_0')/\Delta S$, $Ra = g\alpha\Delta TH^3/\nu\kappa$ is the thermal Rayleigh number, $Rs = g\beta\Delta SH^3/\nu D$ is the solutal Rayleigh number, $Pr = \nu/\kappa$ is the Prandtl number, and $Sc = \nu/D$ is the Schmidt number. Here u and v are the x and y components of the fluid velocity, ψ is the stream function, g is the magnitude of the gravitational acceleration (which is in the negative y direction), ν is the kinematic viscosity, κ is the thermal diffusivity,

and D is the solute diffusivity. Our sign convention is such that both Ra and Rs are positive for the case of a fluid heated and salted from above. In choosing dimensionless units we have used a length scale H and a time scale H^2/ν.

The governing equations admit a quiescent base state ($\psi = 0$) with linear temperature and solute fields, $T = y$ and $S = y$. The boundary conditions chosen to describe this state are $\psi = \partial^2\psi/\partial y^2 = 0$ and $T = S = 1$ for $y = 1$, $\psi = \partial^2\psi/\partial y^2 = T = S = 0$ for $y = 0$, and $\psi = \partial\psi/\partial x = \partial S/\partial x = 0$ and $T = y$ for $x = -L$ and $x = L$.

The equations describing the linear stability of the base state are then

$$-\partial(\nabla^2\tilde{\psi})/\partial t = -\nabla^2(\nabla^2\tilde{\psi}) + (Ra/Pr)(\partial\tilde{T}/\partial x) - (Rs/Sc)(\partial\tilde{S}/\partial x) \quad (4)$$

$$\partial\tilde{T}/\partial t - \partial\tilde{\psi}/\partial x = \nabla^2\tilde{T}/Pr \quad (5)$$

$$\partial\tilde{S}/\partial t - \partial\tilde{\psi}/\partial x = \nabla^2\tilde{S}/Sc \quad (6)$$

with $\tilde{\psi} = \partial^2\tilde{\psi}/\partial y^2 = \tilde{T} = \tilde{S} = 0$ at $y = 0$ and $y = 1$, and $\tilde{\psi} = \partial\tilde{\psi}/\partial x = \partial\tilde{S}/\partial x = \tilde{T} = 0$ at $x = -L$ and $x = L$. Here $\tilde{\psi}$, $\tilde{S}$, and $\tilde{T}$ are perturbations to the base state.

The boundary conditions at $y = 0$ and $y = 1$ are consistent with a y-dependence of the form $\sin(n\pi y)$. We will consider the case with the lowest vertical wavenumber $n = 1$. Indeed, for the particular boundary conditions chosen here, higher values of n simply correspond to several copies of $n = 1$ systems stacked vertically one upon the other, so that knowledge of the $n = 1$ system for all values of the width L therefore includes the behavior for all n as well. We also confine the discussion to the case of "exchange of stabilities;" that is, at the onset of instability we assume that the convection is steady and time-independent. This is known to be true in the simpler case of a laterally infinite domain, and the assumption was also tested numerically in a number of cases for the system discussed here, with no observed oscillatory

behavior. With these assumptions, the governing equations reduce to a set of ordinary differential equations:

$$(D^2 - \pi^2)^2\hat{\psi} = Ra D\hat{T} - Rs D\hat{S} \tag{7}$$

$$-D\hat{\psi} = (D^2 - \pi^2)\hat{T} \tag{8}$$

$$-D\hat{\psi} = (D^2 - \pi^2)\hat{S} \tag{9}$$

for $\hat{\psi}(x)$, $\hat{T}(x)$, and $\hat{S}(x)$, where now $D = d/dx$. The boundary conditions are $\hat{\psi} = D\hat{\psi} = \hat{T} = D\hat{S} = 0$ at $x = -L$ and $x = L$. The Prandtl number Pr and the Schmidt number Sc have been removed from the linear problem by rescaling the temperature and solute field, so that the perturbed temperature and solute fields have the form $\tilde{T}(x,y) = Pr\hat{T}(x)\sin(\pi y)$ and $\tilde{S}(x,y) = Sc\hat{S}(x)\sin(\pi y)$, respectively. The perturbed stream function has the form $\tilde{\psi}(x,y) = \hat{\psi}(x)\sin(\pi y)$. There are therefore just three parameters appearing in the linear problem for the onset of steady convection: the dimensionless half width L, the thermal Rayleigh number Ra, and the solutal Rayleigh number Rs. For given values of L and Ra, we seek the critical solutal Rayleigh number Rs^*, which is the smallest value of Rs for which the governing equations admit a non-trivial solution.

Note that for the case of a laterally-unbounded system, the equations admit periodic solutions $\hat{T} = \hat{S} = k\cos(kx)$, $\hat{\psi} = (k^2 + \pi^2)\sin(kx)$, where the solutal Rayleigh number is then $Rs = Ra + (k^2 + \pi^2)^3/k^2$. The critical solutal Rayleigh number then satisfies $Rs^* - Ra = 27\pi^4/4 \cong 657.5$, and corresponds to a critical wavenumber $k^* = \pi/\sqrt{2}$.

3. A Numerical Approach

The governing equations (7-9) may be rewritten as a set of eight real, coupled, first order linear ordinary differential equations, with the parameter Rs considered as an eigenvalue. As in earlier treatments of eigenvalue problems

described by ordinary differential equations [7], the numerical solution was obtained using the linear boundary value problem software package SUPORT [10]. Following a method described by Keller [11], the homogeneous eigenvalue problem is converted to a nonsingular inhomogeneous problem by altering the form of the boundary conditions so that the solution satisfies, say, $D^3\hat{\psi}(L) = 1$ rather than $\hat{\psi}(L) = 0$. Using SUPORT to solve this problem, the desired solution is obtained by using a nonlinear root solver to vary Rs until the solution satisfies the proper boundary condition $\hat{\psi}(L) = 0$. For most of the calculations the subroutine SNSOE [12,13] was used to find solutions to this equation. The nonlinear root solver PITCON [14] was also used to track solutions by a continuation method to obtain $Rs^*(L)$, the critical Rayleigh number as a function of the half-width L.

4. An Analytical Approach

The set of ordinary differential equations (7-9) has constant coefficients and so admits solutions whose x-dependence is of the form exp(iax), where the wavenumber a may be real or complex. With the assumption $\hat{\psi}(x) = \psi_0 \exp(iax)$, $\hat{T}(x) = T_0 \exp(iax)$, and $\hat{S}(x) = S_0 \exp(iax)$, a solution is obtained provided that a^2 is a root of the fourth-degree polynomial

$$(a^2 + \pi^2)[(a^2 + \pi^2)^3 - a^2\Delta R] = 0 \qquad (10)$$

where $\Delta R = Rs - Ra$. In terms of a^2, there is one root $a^2 = -\pi^2$ and three other roots obtained from the relation $(a^2 + \pi^2)^3 - a^2\Delta R = 0$, which is the same relation that appears for a single-component system [9]. The latter roots a^2 are shown in Fig. 1 as a function of ΔR. There is one root a^2 which is always real and negative, which we will label $-a_3^2$ with $a_3 > 0$. The remaining two roots a^2 may be either real and positive or complex conjugate pairs, depending on whether ΔR is greater than or less than $27\pi^4/4$. For $\Delta R > 27\pi^4/4$,

we label the two roots as $a_1^2 > a_2^2$, with $a_1 > 0$ and $a_2 > 0$. If $\Delta R < 27\pi^4/4$ the two roots are denoted by a_1^2 and a_2^2, where $a_1 = \mu + i\nu$ and $a_2 = a_1^*$, with $\mu > 0$ and $\nu > 0$. The superscript "*" denotes the complex conjugate. For $\Delta R = 27\pi^4/4$, the two roots a_1^2 and a_2^2 become equal, and for $\Delta R = 0$, all three roots a_1^2, a_2^2, and $-a_3^2$ become equal to $-\pi^2$. For these special values of ΔR the degeneracy of the roots forces one to include secular forms, such as $x \exp(iax)$, to obtain linearly independent solutions.

There are therefore eight linearly independent solutions that may generally be obtained from the eight roots for a. Because of the symmetry of the equations and boundary conditions to reflection about the origin x = 0, these solutions may be combined into either even or odd solutions about x = 0 [9]. We denote even solutions as those for which $\hat{T}(x)$ and $\hat{S}(x)$ are even functions of x and the stream function $\hat{\psi}(x)$ is odd; the reverse is true for the odd solutions. Even or odd eigenfunctions are then constructed by expressing the eigenfunction as a sum of the four even or odd linearly independent solutions to the linear ordinary differential equations using four undetermined coefficients. Imposing the boundary conditions $\hat{\psi} = D\hat{\psi} = \hat{T} = D\hat{S} = 0$ at x = L results in a homogeneous system of linear equations for the four unknown coefficients. For non-zero solutions the determinant of the system must vanish, which is the required equation for the solutal Rayleigh number Rs in terms of L and Ra. For the even case, this determinant takes the form

$$\pi Ra T_4(\beta_1 A_1 + \beta_2 A_2 + \beta_3 A_3) \qquad (11)$$
$$-Rs(-\beta_1 a_1 T_1 A_1 - \beta_2 a_2 T_2 A_2 + \beta_3 a_3 T_3 A_3) = 0$$

and for the odd case it has the form

$$\pi Ra(-\beta_1 T_1 B_1 - \beta_2 T_2 B_2 + \beta_3 T_3 B_3) \qquad (12)$$
$$-Rs T_4(-\beta_1 a_1 B_1 - \beta_2 a_2 B_2 + \beta_3 a_3 B_3) = 0$$

where

$$T_1 = \tan(a_1 L)$$
$$T_2 = \tan(a_2 L)$$
$$T_3 = \tanh(a_3 L)$$
$$T_4 = \tanh(\pi L)$$

$$\beta_1 = (\pi^2 + a_1^2)^{-1}$$

$$\beta_2 = (\pi^2 + a_2^2)^{-1}$$

$$\beta_3 = (\pi^2 - a_3^2)^{-1}$$

$$A_1 = (T_2/a_2) - (T_3/a_3)$$
$$A_2 = (T_3/a_3) - (T_1/a_1)$$
$$A_3 = (T_1/a_1) - (T_2/a_2)$$

$$B_1 = (T_3/a_2) + (T_2/a_3)$$
$$B_2 = -(T_1/a_3) - (T_3/a_1)$$
$$B_3 = (T_1/a_2) - (T_2/a_1)$$

Note that the numbers a_1, a_2, and a_3 all depend on the difference $\Delta R = Rs - Ra$. For given values of Ra and L, solutal Rayleigh numbers were computed from these relations using the program ZEROIN by Shampine and Watts [15]. The resulting values of Rs agreed with those values obtained from the numerical solution of equations (7-9) to within the assigned tolerances (usually five digits). As discussed below we also examine the asymptotic behavior for large widths $L \gg 1$, and $\Delta R < 27\pi^4/4$, in which case we have $T_1 \equiv i$, $T_2 \equiv -i$, and $T_3 \equiv T_4 \equiv 1$, and the two determinants become equal.

5. Results

In Figures 2 and 3 we give marginal stability results as a function of the width 2L for Ra = 0 and Ra = 3000, respectively. The results are given in terms of ΔR in order to facilitate comparison with the laterally-unbounded case, for which $\Delta R^* = Rs^* - Ra = 27\pi^4/4$, independent of the value of Ra. In both figures several curves are shown, corresponding to the lowest two even and odd modes in each case. The critical value ΔR^* then corresponds to the lowest value of ΔR for each width. For Ra = 0 (Figure 2), the thermal

field contributes no driving force to the flow and the flow corresponds to that for a single component. These curves therefore reproduce results of Drazin [9], Hall and Walton [16], and Daniels [17]. In particular, Rs^* approaches the asymptotic value of $27\pi^4/4$ as L becomes infinite. That is, for the single component case, as the distance between sidewalls becomes larger and larger, they have less and less of an effect, and the stability of the system is approximated more and more closely by that for the laterally unbounded case, for which $Rs^* = 27\pi^4/4$. Roughly speaking, the variation in Rs^* for finite L is due to the fact that a set of rolls with preferred wavelength $2\pi/k^* = 2\sqrt{2}$ cannot exactly fit between the walls and still satisfy the proper boundary conditions, so that a modulation of the wavenumber over the length L is required, which also causes an increase in Rs^*.

For Ra = 3000 (Figure 3) the asymptotic value of ΔR^* for large L is about 50, which is well below the value for a laterally unbounded system. As will be discussed shortly, this destabilization becomes even more pronounced as Ra increases, with the asymptotic values of ΔR^* tending to minus infinity as $Ra \to \infty$. Thus for the two-component system the sidewalls do not have less and less of an effect as the width of the system becomes larger and larger.

It can easily be shown that the destablization relative to the single component case is related to the fact that T and S satisfy different boundary conditions. Indeed, if they satisfied the same boundary conditions, then by subtracting equation (9) from (8) it can be seen that the difference $\hat{S}(x) - \hat{T}(x)$ satisfies $(D^2 - \pi^2)(\hat{S} - \hat{T}) = 0$ with homogeneous boundary conditions, and so must vanish identically. Eliminating $\hat{T}(x)$ from Eqs. (7-9) then results in equations describing a system with a single destabilizing component with an effective Rayleigh number Rs - Ra, for which the asymptotic limit for large

L is $27\pi^4/4$. Figure 2 can therefore be interpreted in two ways. It gives Rs versus width (2L) for the single component system with Ra = 0 as shown, or, equivalently, it gives ΔR versus width for a two-component system with matching boundary conditions on the sidewalls (both perfectly insulating in this case).

Thus for Ra = 3000, we may consider Figures 2 and 3 to represent the cases of thermally insulating and thermally conducting sidewalls, respectively. We may continuously pass from one case to the other by writing the thermal boundary conditions in the form

$$\cos(\phi)\hat{T}(L) + \sin(\phi)D\hat{T}(L) = 0$$

$$\cos(\phi)\hat{T}(-L) - \sin(\phi)D\hat{T}(-L) = 0,$$

for $0 \leq \phi \leq \pi/2$. The behavior of the two lowest ("destabilized") modes in Figure 3 may be observed as the boundary conditions change. In Figure 4 we show the change in ΔR with ϕ for a width 2L = 4.0 for the three lowest odd modes. All three modes show a decrease in ΔR as ϕ ranges from $\pi/2$ (thermally insulating) to zero (thermally conducting) and the relative order of the modes is preserved. The lowest mode shows a much larger change as $\phi \to 0$. The lower two modes in Figure 4 correspond to the two odd modes shown in each of Figures 2 and 3. We see from Figure 4 that ΔR varies continuously with ϕ. Only the first pair of even and odd modes in Figure 2 are destabilized to values $\Delta R < 27\pi^4/4$ as Ra increases (Figure 3); the second pair of modes apparently still asymptote to $\Delta R = 27\pi^4/4$ as $L \to \infty$.

The lowest curve in Figure 3 does not descend to its asymptotic value as L increases, but shows a minimum value of $\Delta R^* = -420$ near 2L = 1.5. For widths larger than this value, therefore, decreasing the separation of the sidewalls results in a significant destabilization of the system. In Figure

5 additional results are given for Rs^* as a function of Ra for 2L = 0.5, 1.0, 1.5, and 2.0. These values for 2L are less than the critical wavelength 2.8 for an unbounded single component system. For $Ra = 10^5$ and 2L = 0.5, $Rs^* \equiv 4.4(10^4)$ or $\Delta R^* \equiv -5.6(10^4)$ indicating that the magnitude of ΔR^* increases with increasing Ra. For large L, this behavior can be described analytically and will be discussed below. Note that the 2L = 1.5 and 2.0 curves cross at $Ra \equiv 10^3$ so that there is a range of Ra values for which the 2L = 1.5 case is less stable than the 2L = 2.0 case. Clearly for sufficiently small L, as indicated by the 2L = 0.5 curve, significant stabilization occurs.

It is clear, then, that for $\hat{T} = D\hat{S} = 0$ on the sidewalls, the critical solutal Rayleigh number does not approach that for an infinite system without sidewalls as the system becomes larger and larger. Examination of the eigenfunctions shows that, for large thermal Rayleigh numbers, most of the flow occurs in a neighborhood of the walls, cf. Figure 6, in a manner suggestive of a buoyancy layer near a heated wall [3]. Thus for large L the interior of the region is relatively free from convection, whereas in the single-component system the interior is filled with an array of convection cells having more or less equal strength, cf. Figure 7. In view of this, an alternative interpretation of the large L limit can be obtained by fixing the left hand boundary, for example by setting $\tilde{x} = x + L$, and then letting the right hand boundary recede to positive infinity while keeping the left hand boundary at $\tilde{x} = 0$. With this change of variables, both the even solutions and the odd solutions tend to the same set of solutions as $L \to \infty$; namely, those for an infinite half-interval with exponential decay as $\tilde{x} \to \infty$ (for $\Delta R < 27\pi^4/4$). These four solutions have spatial variations given by

$$F_1(\tilde{x}) = \exp(ia_1\tilde{x})$$

$$F_2(\tilde{x}) = \exp(-ia_2\tilde{x})$$

$$F_3(\tilde{x}) = \exp(-a_3\tilde{x})$$

$$F_4(\tilde{x}) = \exp(-\pi\tilde{x})$$

and the characteristic determinant derived from the boundary conditions at $\tilde{x} = 0$ is then

$$\pi Ra\{\beta_1(-i/a_2 - 1/a_3) + \beta_2(1/a_3 - i/a_1) + \beta_3(i/a_1 + i/a_2)\} \qquad (13)$$

$$-Rs\{-i\beta_1 a_1(-i/a_2 - 1/a_3) + i\beta_2 a_2(1/a_3 - i/a_1) + \beta_3 a_3(i/a_1 + i/a_2)\} = 0$$

which is the large l limit of both equation (11) and equation (12). For large but finite L, therefore, the exponential decay of the eigenfunctions with distance from the wall means that there are basically two isolated regions of flow, each located near one of the walls, each of which approaches the limiting case of flow in a semi-infinite slab as the sidewall separation becomes large.

For L infinite we have also considered the asymptotic dependence of the critical solutal Rayleigh number Rs^* on Ra for large Ra. This involves deriving an expansion of the roots a^2 for $-\Delta R >> 1$, inserting them into the determinant (13), and again expanding for $Ra >> 1$. The calculations were carried out using the symbol manipulation software MACSYMA [18], with the result being

$$Rs = 2\pi Ra^{3/4}\{1 + (3/\sqrt{8})\pi Ra^{-1/4} + (15/16)\pi^2 Ra^{-1/2} + O(Ra^{-3/4})\} \qquad (14)$$

The dependence on $Ra^{1/4}$ is also characteristic of the width of the long narrow cells that occur in the fingering regime [3,6]. An intermediate result is that $a_3 \sim \pi^3/Ra^{1/2}$, and the fact that a_3 tends to zero as $Ra \to \infty$ causes a slowly decaying tail of the disturbance to extend to the interior of the region for large Ra.

For large L, the flow is confined to the neighborhood of the walls as

illustrated in Figure 6. Since the flow near one wall is essentially independent of the flow near the other wall, the critical value of the solutal Rayleigh number is nearly the same for even and odd modes (see Figure 3). The local flow adjacent to each wall is in opposite directions for the odd mode (see Figure 6) and is in the same direction for the even mode. As the separation of the walls decreases, the localized flows begin to interact and the critical Rayleigh numbers for the even and odd modes become increasingly different. As shown in Figures 8 and 9 for 2L = 3.0 and 1.5, for the odd mode the interaction tends to weaken the flow in the interior whereas for the even mode the flow in the interior is reinforced. The even mode consists of two convection cells separated by a dividing vertical streamline midway between the walls. The odd mode undergoes a transition from a flow with essentially two cells (Figure 6) to a mixed flow with a dividing separatrix at the center of the region (Figure 8) to a single unicell (Figure 9) as L decreases. The difference between the critical solutal Rayleigh numbers for the even and odd mode is 134 and 1747 for 2L = 3.0 and 1.5, respectively. Thus, for 2L = 1.5, the unicell is significantly less stable than the two cell structure.

6. Conclusions

In the presence of sidewalls the critical solutal Rayleigh number Rs^* for convective instability can be significantly lower than that for a laterally unbounded system. The flow in the unbounded system consists of a periodic array of convection cells of equal strength, whereas the presence of sidewalls allows a localized flow to develop near the walls at a significantly lower solutal Rayleigh number. Maximum destabilization occurs for a finite value of L.

The stability of the finite system is sensitive to the particular form of the boundary conditions imposed on the sidewalls. Changing the thermal

boundary conditions from conducting to insulating stabilizes the system (and considerably alters the nature of the flow in the interior of the system at the onset of instability). This effect is consistent with the statement that the change from Neumann to Dirichlet boundary conditions for the temperature field has the effect of imposing a constraint on the temperature field, which is therefore less effective in stabilizing the flow field.

7. Acknowledgements

This work was conducted with the support of the Microgravity Sciences Program, National Aeronautics and Space Administration. A portion of the work was performed while one of the authors (GBM) was visiting the Institute for Theoretical Physics, University of California Santa Barbara, whose hospitality is gratefully acknowledged. We also thank R. F. Sekerka for helpful discussions.

References

1. H. Stommel, A. B. Arrons, and D. Blanchard, Deep-Sea Res. 3, 152 (1956).

2. H. E. Huppert and J. S. Turner, J. Fluid Mech. 106, 299 (1981).

3. J. S. Turner, Buoyancy Effects in Fluids, Cambridge University Press, New York, NY, 1973.

4. J. S. Turner, Ann. Rev. Fluid Mech. 6, 37 (1974).

5. C. F. Chen and D. H. Johnson, J. Fluid Mech. 138, 405 (1984).

6. M. E. Stern, Tellus 12, 172 (1960).

7. S. R. Coriell, M. R. Cordes, W. J. Boettinger, and R. F. Sekerka, J. Crystal Growth 49, 13 (1980).

8. G. B. McFadden, R. G. Rehm, S. R. Coriell, W. Chuck, and K. A. Morrish, Metall. Trans. 15A, 2125 (1984).

9. P. G. Drazin, Z. angew. Math. Phys. 26, 239 (1975).

10. M. R. Scott and H. A. Watts, SIAM J. Numerical Anal. 14, 40 (1977).

11. H. B. Keller, Numerical Solution of Two Point Boundary Value Problems, Regional Conference Series in Applied Mathematics, SIAM, Philadelphia, PA, 1976, vol. 24.

12. SLATEC Common Math Library, National Energy Software Center, Argonne National Laboratory, Argonne, IL. SNSQE was written by K. Hiebert (1980), based on Powell [13].

13. M. J. D. Powell, Numerical Methods for Nonlinear Algebraic Equations. P. Rabinowitz, ed., Gordon and Breach, New York, NY, 1970, 87.

14. W. C. Rheinboldt and J. V. Burkardt, ACM Trans. Math. Software 9, 215 (1983).

15. L. Shampine and R. C. Allen, Jr., Numerical Computing: An Introduction, W. B. Saunders & Co., Philadelphia, PA, 1973.

16. P. Hall and I. C. Walton, Proc. Roy. Soc. Lond. A. 358, 199 (1977).

17. P. G. Daniels, Z. angew. Math. Phys. 28, 577 (1977).

18. MACSYMA Reference Manual, Version 10, 1983. By the Mathlib Group - Room 832, Laboratory for Computer Science, Massachusetts Institute of Technology, 545 Technology Square, Cambridge, MA 02139.

Figure Captions

Figure 1. The real and imaginary parts of the roots a^2 of the cubic equation $(a^2 + \pi^2)^3 - a^2\Delta R = 0$. The dashed curve indicates the real part of two complex conjugate roots.

Figure 2. The values $\Delta R = Rs - Ra$ for $Ra = 0$ as a function of dimensionless width for $\hat{T} = D\hat{S} = 0$ on the lateral walls. The ΔR curves for any values of Ra with $D\hat{T} = D\hat{S} = 0$ on the lateral walls are identical to these curves.

Figure 3. The values $\Delta R = Rs - Ra$ for $Ra = 3000$ as a function of dimensionless width for $\hat{T} = D\hat{S} = 0$ on the lateral walls.

Figure 4. Dependence of $\Delta R = Rs - Ra$ on the thermal boundary conditions for the lowest three odd modes with $Ra = 3000$ and $L = 2.0$. Here the thermal boundary conditions on the lateral walls have the form $\cos(\phi)\hat{T}(L) + \sin(\phi)D\hat{T}(L) = 0$ and $\cos(\phi)\hat{T}(-L) - \sin(\phi)D\hat{T}(-L) = 0$.

Figure 5. The critical solutal Rayleigh number Rs^* as a function of thermal Rayleigh number Ra for widths of 0.5, 1.0, 1.5, and 2.0.

Figure 6. The variation with x of the eigenfunctions $\hat{\psi}$, $\hat{S}$, and $\hat{T}$ for $Ra = 3000$ and a width of ten with $\hat{T} = D\hat{S} = 0$ on the walls corresponding to a critical value of $\Delta R^* = Rs^* - Ra = 46.4$. Also shown is a contour plot of the stream function $\hat{\psi}(x)\sin(\pi y)$ with contour spacings of 0.25.

Figure 7. The variation with x of the eigenfunctions $\hat{\psi}$, $\hat{S}$, and $\hat{T}$ for a width of ten with $D\hat{T} = D\hat{S} = 0$ on the walls corresponding to a critical value of $\Delta R^* = Rs^* - Ra = 671.3$. Also shown is a contour plot of the stream function $\hat{\psi}(x)\sin(\pi y)$ with contour spacings of 0.25; solid and dashed curves indicate positive and negative values, respectively. For these boundary conditions ΔR is independent of Ra.

Figure 8. Spatial variation of the stream function for $Ra = 3000$ and a width of three with $\hat{T} = D\hat{S} = 0$ on the walls. The lowest even (upper plot) and odd (lower plot) modes are shown corresponding to $\Delta R = Rs - Ra = 99.3$ and -34.7, respectively.

Figure 9. Spatial variation of the stream function for $Ra = 3000$ and a width of 1.5 with $\hat{T} = D\hat{S} = 0$ on the walls. The lowest even (upper plot) and odd (lower plot) modes are shown corresponding to $\Delta R = 1331.1$ and -415.7, respectively.

Figure 1

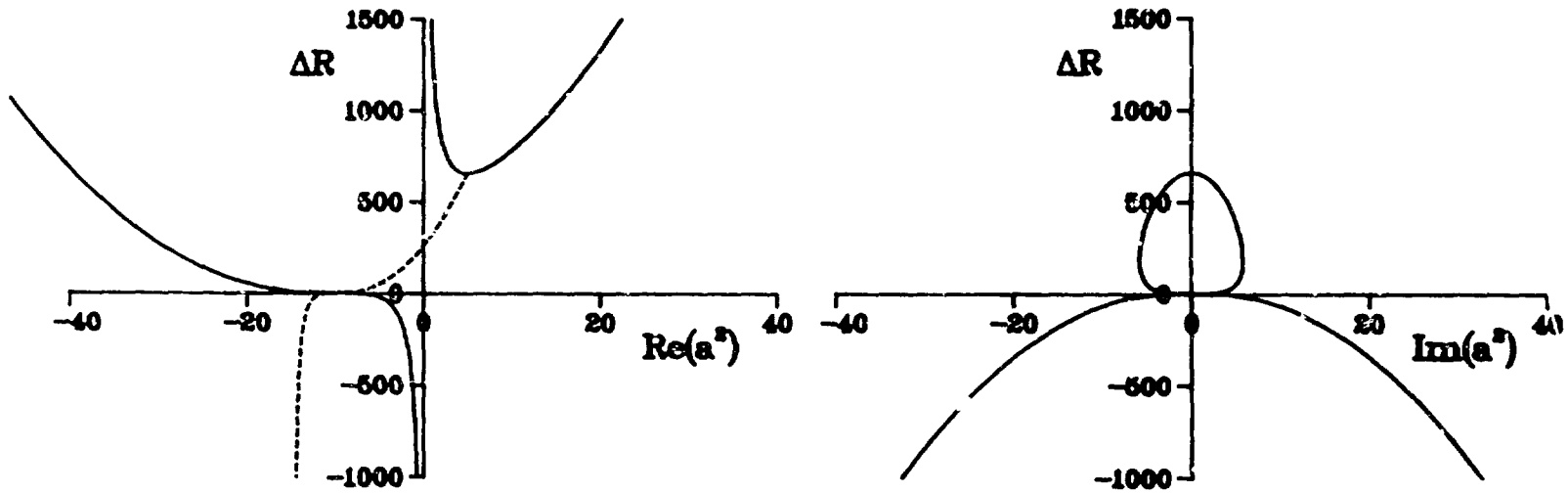
ΔR
1500
1000
500
-500
-1000
-40
-20
0
20
40
Re(a²)
ΔR
1500
1000
500
-500
-1000
-40
-20
0
20
Im(a²)

Figure 2

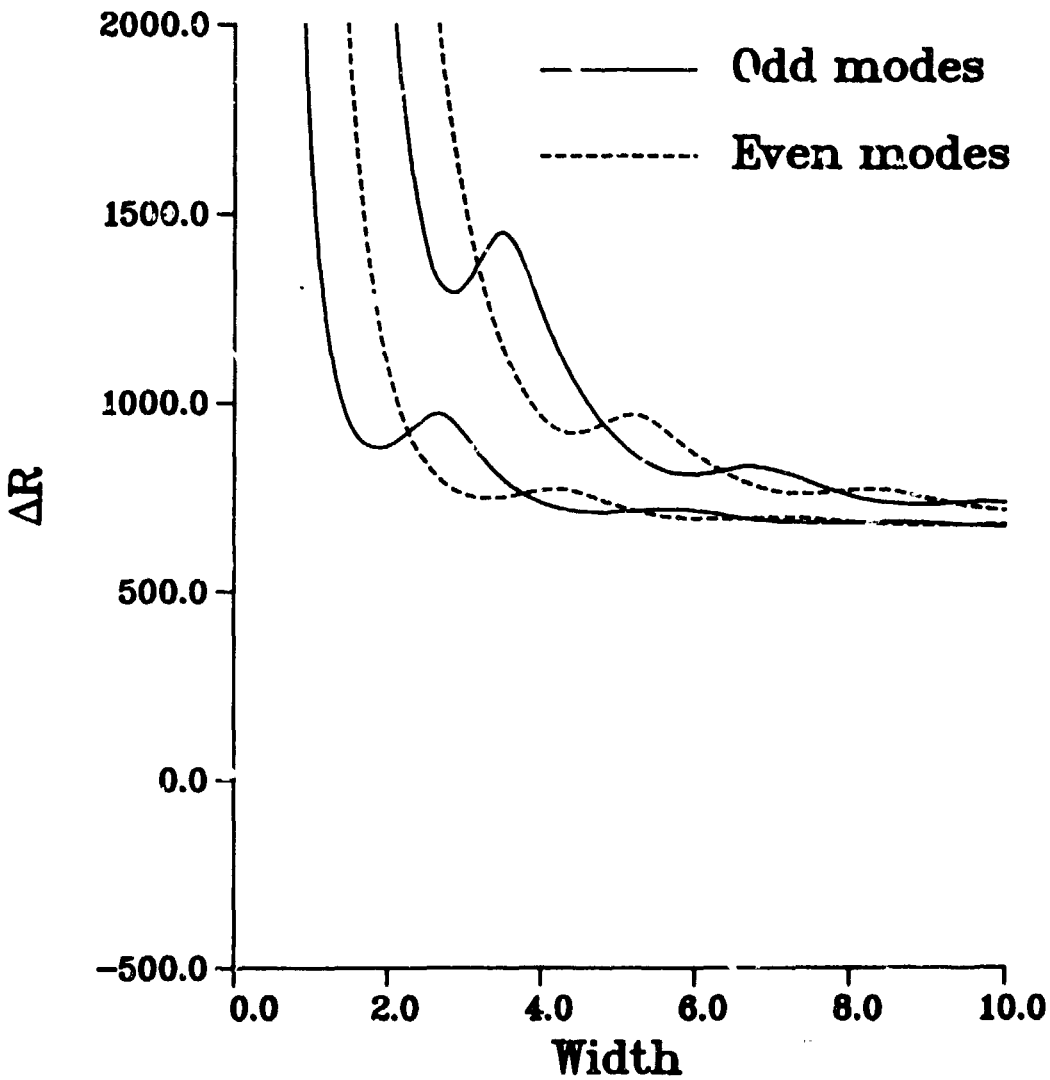
2000.0
1500.0
1000.0
500.0
0.0
-500.0
ΔR
0.0
2.0
4.0
6.0
8.0
10.0
Width
Odd modes
Even modes

Figure 3

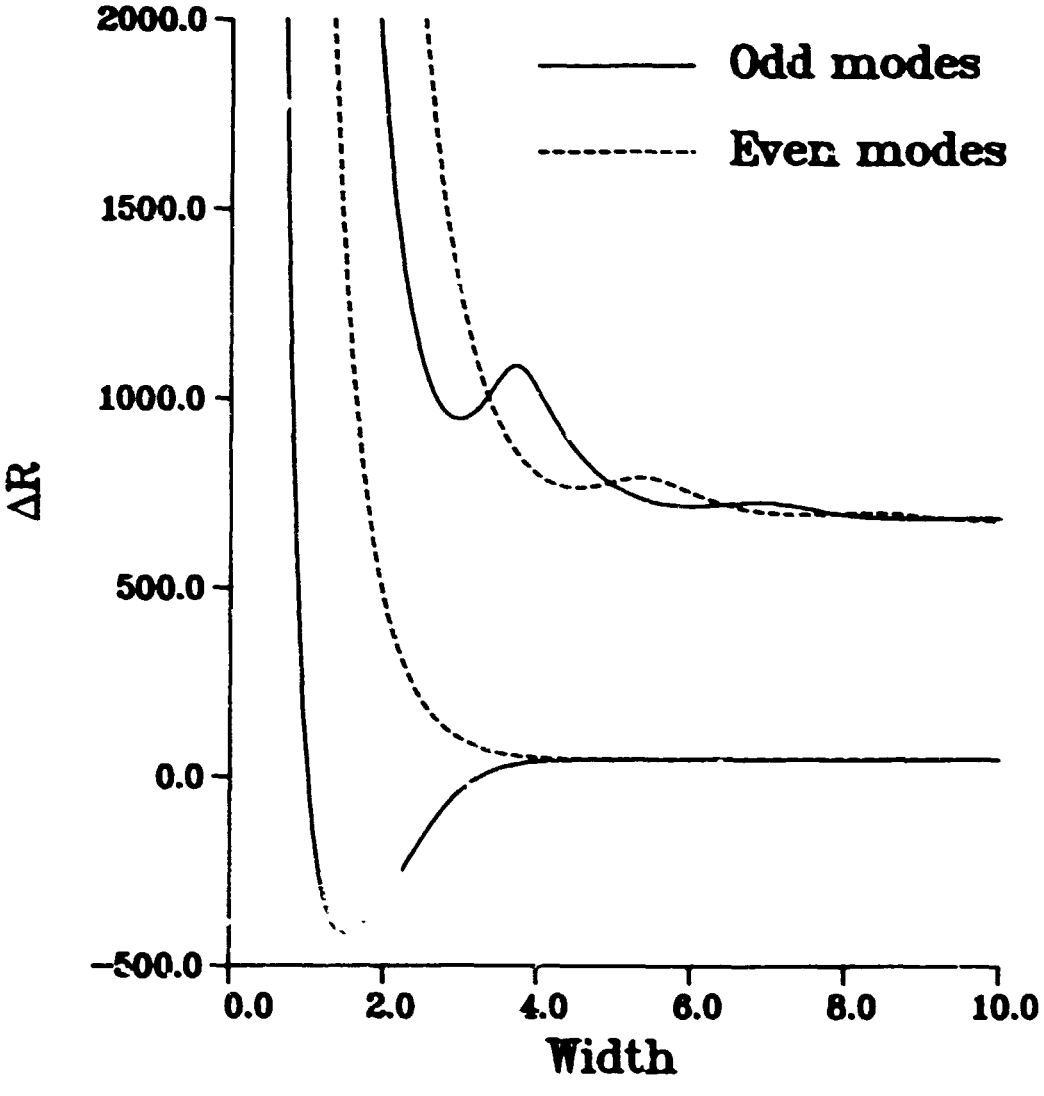
2000.0
1500.0
1000.0
500.0
0.0
-500.0
ΔR
0.0
2.0
4.0
6.0
8.0
10.0
Width
Odd modes
Even modes

Figure 4

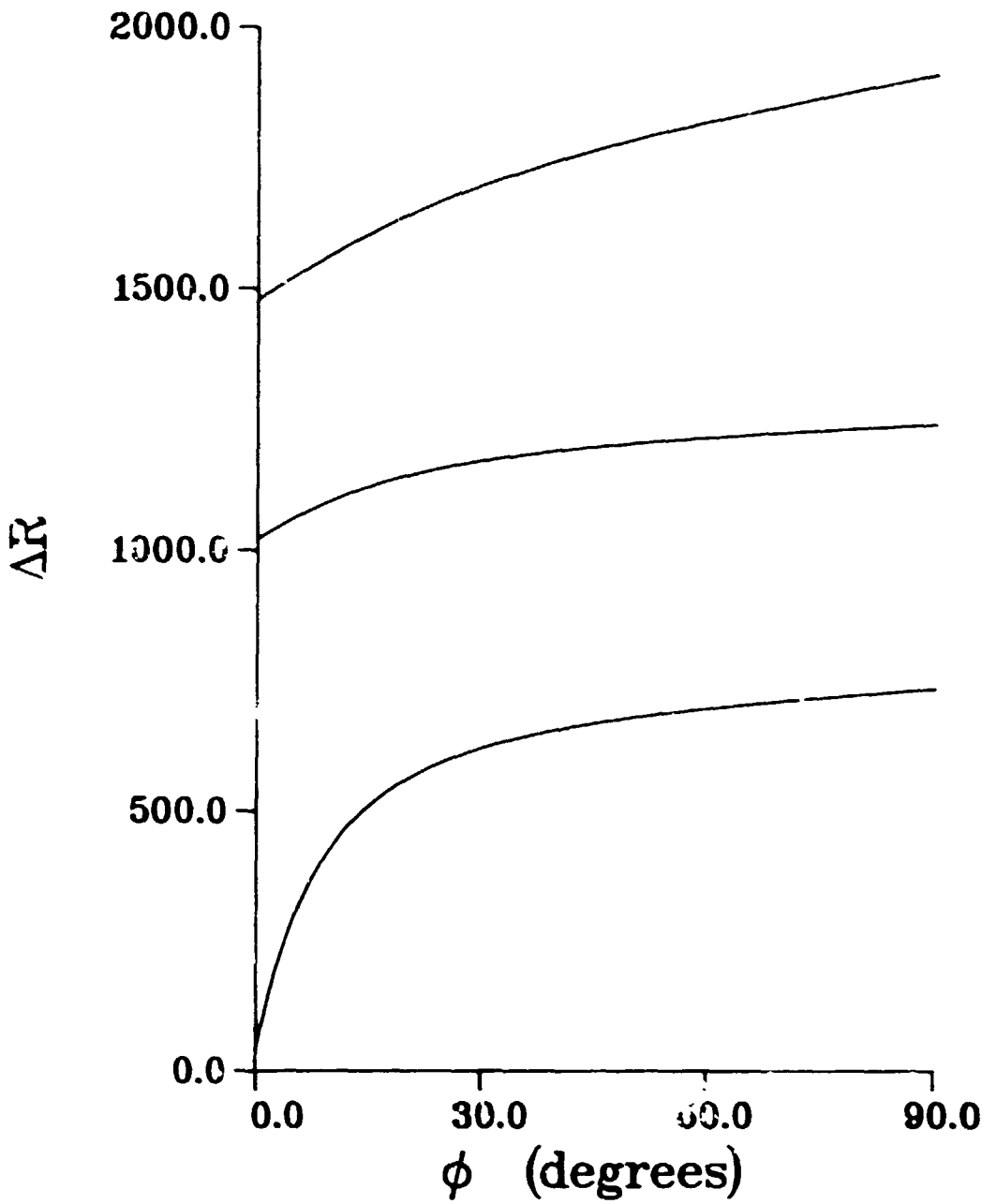

Figure 5

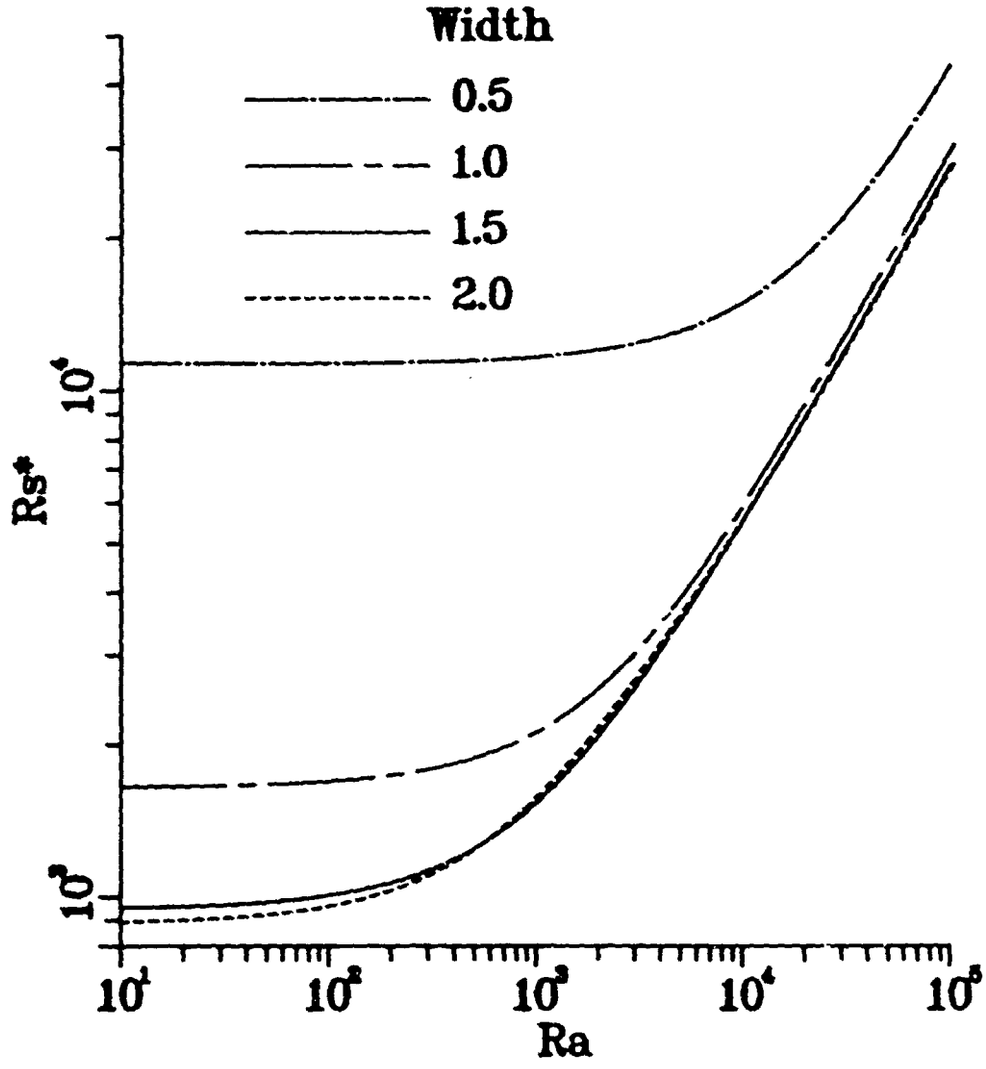

Figure 6

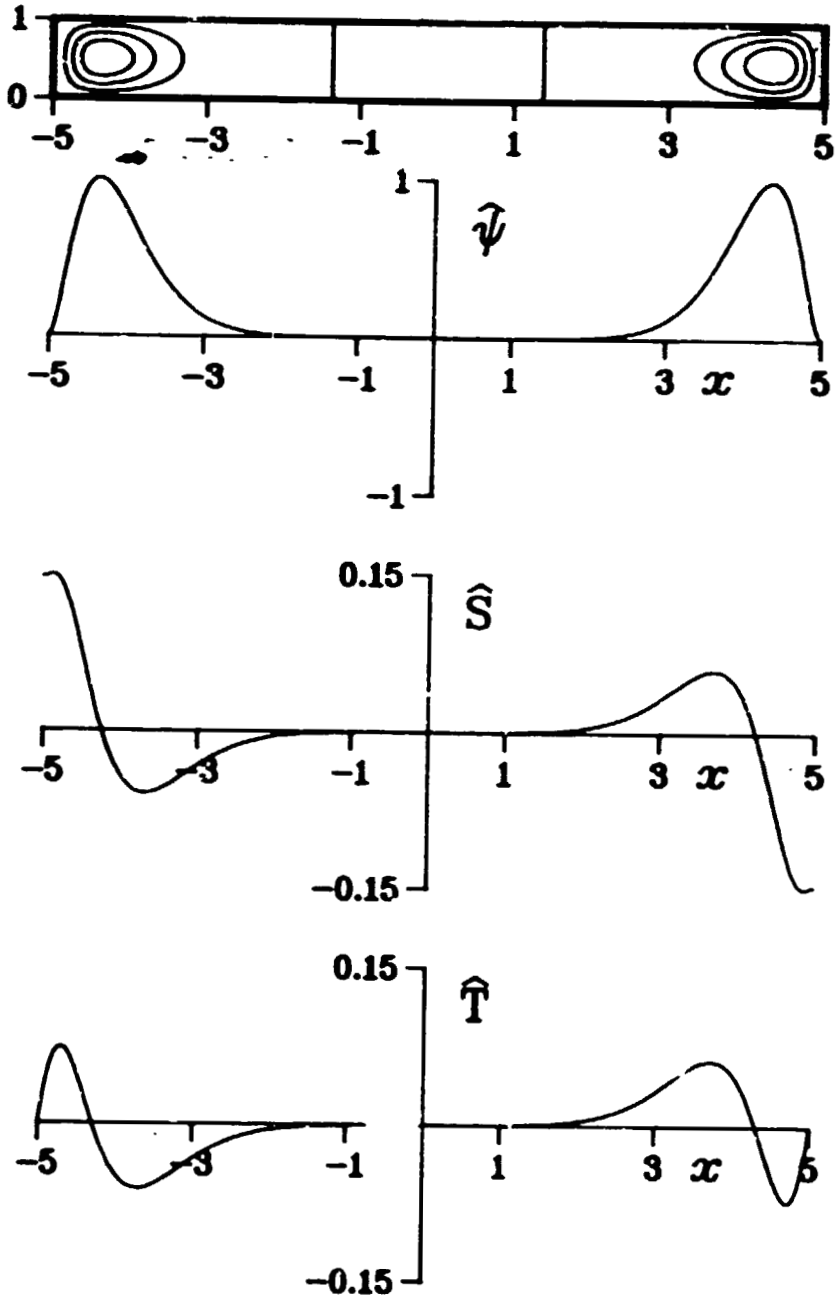

Figure 7

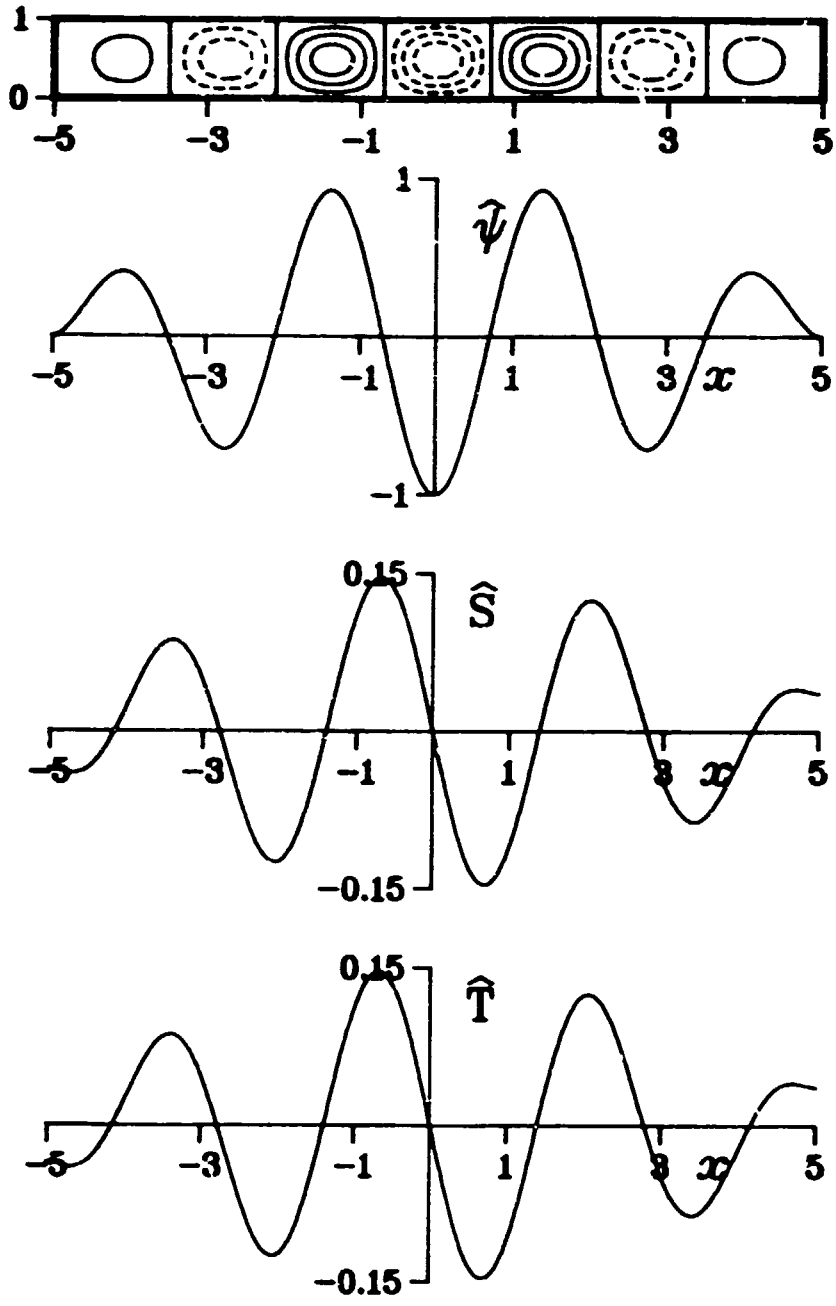
1
0
-5
-3
-1
1
3
5
1
$\hat{\psi}$
-5
-3
-1
1
3
x
5
-1
0.15
$\hat{S}$
-5
-3
-1
1
3
x
5
-0.15
0.15
$\hat{T}$
-5
-3
-1
1
3
x
5
-0.15

Figure 8

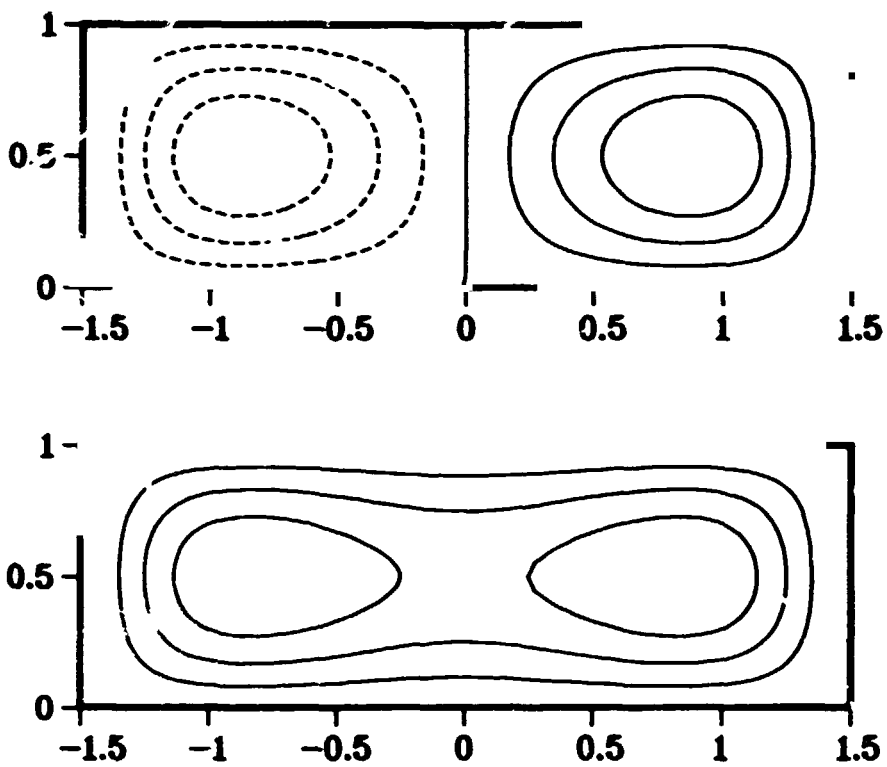

Figure 9

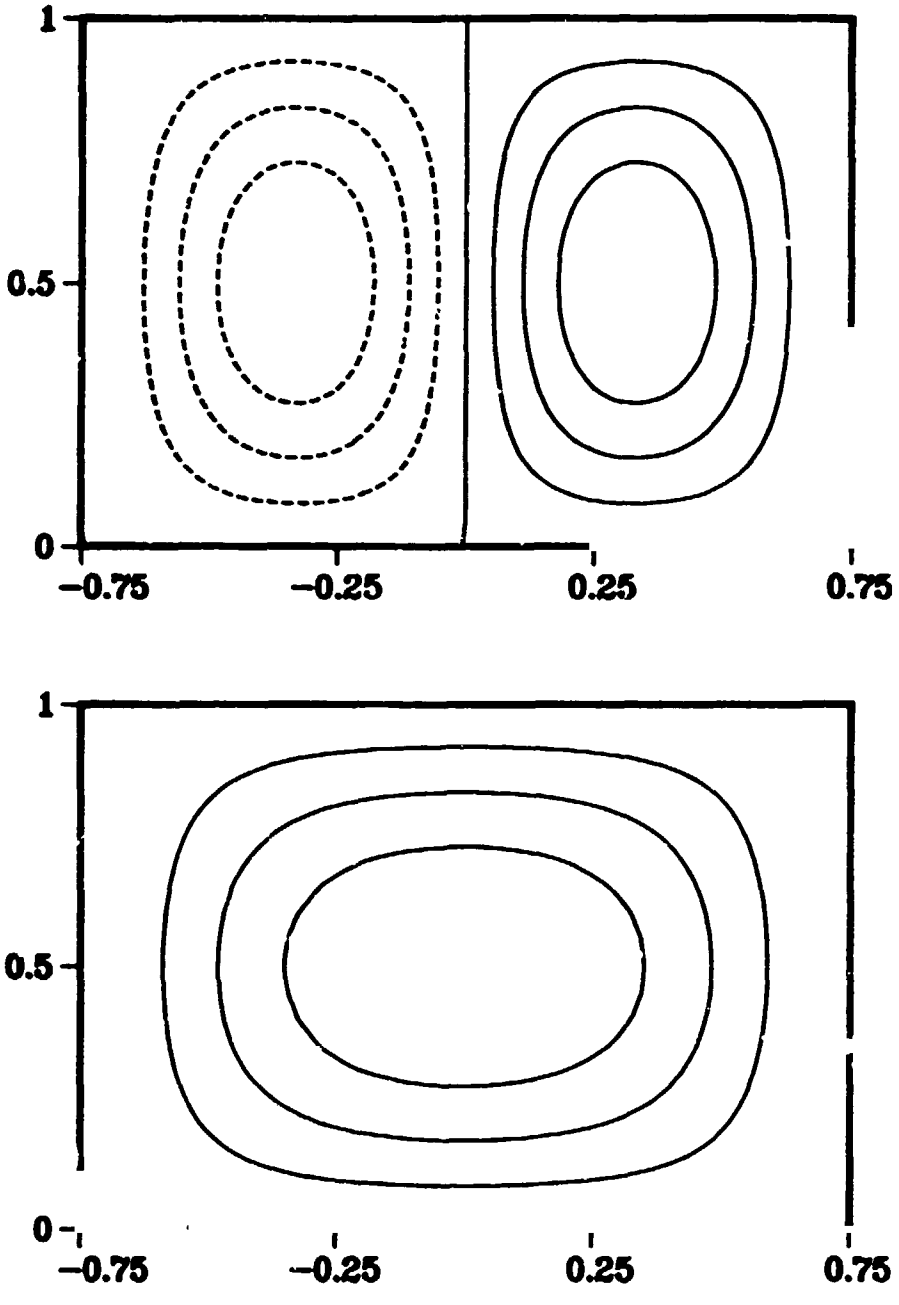

Task 3

Measurement of High Temperature Thermodynamic Properties

D. W. Bonnell

SUMMARY

Major efforts in the interaction between Rice University (RICE), the General Electric Space Facilities Laboratory (GE) and the National Bureau of Standards (NBS) through this project have concentrated in two areas over the past year. The first area is the prototyping of software on a portable computer, suitable for transporting to the experimental site which would provide both data acquisit on and data reduction, independent of the need to rely on external computers or data transmission to ascertain the current state of the experiment. This effort is intended to provide support both to the on-going ground-based experimental effort in levitation calorimetry, and also to act as the prototype for flight experiments. The second effort has been the exploration of experimental flight opportunities in the area of high temperature properties measurements. D. W. Bonnell has been selected as a member of the "High Temperature Advisory Committee", a NASA sponsored group, which met at the Jet Propulsion Laboratory (JPL) in February of 1985 to consider the general requirements of high temperature utilization of microgravity, and to provide scientific guidance to the JPL levitation research, particularly use of acoustic techniques. A visit to RICE in March of 1985 was made to discuss flight experiment possibilities, to discuss current ground-based efforts and examine current experimental arrangements, and to discuss automation access. The results of these efforts suggest that there is potential for flight experimental work, although the applicability of acoustic positioning in significant high temperature efforts is yet to be established. Silicon

metal seems to be a good candidate, since it is extremely reactive, very difficult to levitate in a one gravity environment, and apparently possesses the highest heat of fusion of any element. A variety of experiments, including volume change on melting, density, and cooling curve heat capacity measurements appear within the current or projected capabilities of hardware being developed for flight (e.g., the GE electromagnetic package).

Introduction

For the past several years, an experimental interaction among workers at General Electric Space Facilities Laboratory (GE, R. T. Frost), Rice University (RICE, J. L. Margrave), and the National Bureau of Standards (NBS, D. W. Bonnell) has been carried out with the purpose of exploring the limits of ground-based high temperature levitation research. This work developed an ultra-high temperature calorimeter system which yielded the first precision value for the heat of fusion of tungsten [Bonnell, 1983]. The levitation system was not really capable of the stable levitation of liquid tungsten necessary for calorimetry of the liquid, but provided a test bed to examine techniques needed for high temperature calorimetry, such as automatic multi-color imaging pyrometry [Bonnell, 1984 and Bonnell, 1982], and other aspects of high temperature calorimetry. This work has culminated in the publication of a review chapter on the subject, Levitation Calorimetry [Bonnell, et al 1985]. One of the aspects of calorimetry brought out by the need to move disparate groups and laboratory equipment to a distant site is the fact that calorimetric studies are generally deliberate, meticulous research, and the apparatus and techniques which have been developed over the years for determinations in such an environment are not necessarily the most effective in a remote environment situation. Since flight experiments will have needs

for immediate data evaluation and response similar to those of the RICE-GE-NBS interaction, this seemed an appropriate time to begin development of a prototype data acquisition and analysis system which supports the experimentalist in data acquisition, and provide local data evaluation to reduce lag in identifying experimental problems. In the past, data has simply been collected without real-time evaluation, and processed later by remote transmission and batch calculation. With the advent of self-contained portable computers supporting high level languages, an evaluation of prototyping languages and codes nas been undertaken.

Because Shuttle-based high temperature microgravity experimental facilities and opportunities will soon be available, research with scientific goals (as opposed to methodology development goals) can now consider the microgravity environment as another viable means of pursuing those goals. In high temperature research efforts, it is still the case that problems utilizing microgravity must be very carefully selected, and that the process of developing experiments must still recognize the infancy of scientific experimentation in space, and be designed accordingly. In particular, the experimental aspects should include relatively simple measurements to be made in early experiments, with only one or two variables to be measured, and have straightforward environmental conditions to be satisfied. The measurements should have high probability of success even with marginal apparatus performance. A third criterion should be that an experimental series should be designed to test, in earlier phases, the apparatus performance which will be needed in later phases. High temperature flight experiments should be selected, keeping in mind these requirements and the current restrictions of upper temperature limits of 1500 to 2000 K, the availability of perhaps 1% temperature precision at best, a

limited multisample capability, and limited operator interaction.

Flight Experimental Opportunities

Although one important class of experiments that would benefit directly from microgravity are the determination of basic thermodynamic data such as fusion heats and heat capacity/enthalpy functions, these experiments require overall precision better than 1-2 percent to be of real value, and generally require several parameters of the system to be measured or controlled. An ideal begining experiment would require only optical access to the sample, should allow the sample to be reused during the flight for multiple determinations, and should yield data for which approximately correct estimates already exist.

Of intrinsic importance, as well as being important parameters in ground-based high temperature determinations, are the density of the liquid, and the volume change on melting. In many cases above 1500 K, the densities of liquid metals are known only approximately, and the general best representation of the temperature dependence is a linear function [Metals Reference Book, 1976]. This representation is heavily weighted by high accuracy low temperature measurements (e.g, Hg), and by the available precision of the high temperature data. In microgravity, surface tension will quickly force a molten sample into a spherical shape, and the requisite positioning forces should distort this sphericity only slightly. Observing a sample as it cools with a dimensionally-calibrated recording optical system (either video or film camera) will readily allow determination of the sample volume from its physical dimensions. This technique has been attempted in ground-based research [Bonnell and Margrave, 1974] with mixed success. In earth-based experiments, the sample is strongly distorted into a "pear" shape by the combination of

gravity and the electromagnetic support fields. One dimensional imaging, with the assumption the specimen was a figure of revolution about the vertical axis limits accuracy to a few percent. As the total change in density upon melting is typically of the order of 10 percent, it is clear that levitation-based techniques need improvement. The volume change on melting is an important parameter itself, being generally larger than the volume change over the useful liquidus temperature range. Measurement of this parameter requires only a just molten sample. Thus, data for this property is an excellent minimal apparatus performance target.

Current density work at RICE will use a mirror arrangement to give 3 orthogonal views, which should improve volume measurement accuracy to the order of 1-2 percent, although in earth gravity, this is an ambitious effort. To improve on this error level in a microgravity experiment should be much easier. A 1% error level for a 1 cm diameter sample corresponds to 3 axis radii measurements precise to 0.02 mm for a sphere. As long as the sample sphericity error is of this order, amounting to about 0.08 eccentricity, corrections to the spherical measurements should contribute with less than 1 percent uncertainty. In earth gravity, eccentricities of the order of 0.85 (2 to 1 axes ratio) are comm , requiring large non-sphericity corrections. In the microgravity environment, one would expect excellent sphericity for a suspended liquid, so that the limiting parameters are optical resolution and sample vibrations, both harmonic and rotational. There are still problems with the sample moving rapidly under the influence of the electromagnetic field (vibrating, spinning, stirring of the melt, etc.) which can limit total precision. In the microgravity environment, the field can be reduced to a level just sufficient for positioning after the sample reaches high temperature.

Spinning, which would produce centrifugal distortions, can be controlled by introducing a deliberate vertical asymmetry in the levitation coil.

This experiment gives directly the temperature dependence of density for very little additional effort over that necessary to simply test levitation and temperature measurement capability. It is not highly dependent on accurate positioning of the specimen, and shows a clear advantage for microgravity measurements. Assuming a calibrated pyrometric or even a moderately bandwidth limited radiance detector, the shape of the light output data during cooling will yield the functional dependence of the high temperature liquid density with temperature.

Cooling Curve Cp Measurements

The next stage in such an experimental series would be to include a relatively high speed 1 or 2 color imaging pyrometer system with 0.5 % or better accuracy, and to monitor the rate of heat loss during cooling to obtain heat capacity (Cp), Weingarten, et al [1977]. Although a much more demanding experiment in terms of system control, this technique represents the next phase of effectively utilizing the microgravity environment. When the completion of a series of density and cooling-function heat capacity experiments have eliminated experimental problems associated with flight microgravity heating and positioning, temperature measurement, and specimen changing, it will be appropriate to consider high precision calorimetric studies, perhaps utilizing a "gulp" calorimeter system similar to that prototyped by GE and recently tested [Frost and Stockoff, 1983; Bonnell, 1983].

Levitation Systems

The recent meeting of the High Temperature Advisory Committee at JPL provided a review of acoustic positioning technology [Doremus, 1985]. These

systems are quite attractive for manipulating non-conductors, e.g., ceramic and glass materials. However, in the ceramics area, materials are generally less reactive and more tractable for earth-bound measurement up to temperatures well above 1800 K. This was pointed out to the JPL staff by the committee, with the recommendation that JPL plan soon to attempt design and development efforts for a high temperature acoustic positioning system to operate above 2300 K, probably based on the single-mode acoustic levitator described by Barmatz [1985] using a compact YAG laser to heat samples of less than 1 mm diameter. It was the committee's opinion that avoiding the problem of heating an entire levitator to temperatures above 2300 K would eliminate a variety of serious problems in the implementation, including heat rejection, total power required, early apparatus failure, hot wall outgas contamination of the sample, etc. The apparatus failure problem, particularly at launch, and the likelihood that a hot container's walls could cause more contamination than levitation would eliminate are powerful arguments in favor of a localized heating arrangement. There are major problems associated with stable levitation in the presence of large gas temperature gradients which need to be investigated and overcome, and the acoustic positioning effect may cause undesirable circulation near the sample, but such problems seem to be development problems, amenable to engineering solutions. The advantages of using acoustic positioning extends research opportunities to ceramics, glasses, molten salts, and other refractory non-conductors.

Although acoustic positioning obviously has significant implications for the future of high temperature space experimentation, it appears that current planning should consider electromagnetic levitation the most probable near term high temperature technique available, thus limiting opportunities to

conductors. Frost [1985] of GE indicates that an electromagnetic levitator system with optical image recording and pyrometry, based in part on the SPAR levitation system used for beryllium in the late 1970's [Wouch, et al, 1978] will be available in the near future with capability of temperatures to the order of 2000 K.

Sample Choice

With this temperature capability, it is practical to consider systems with melting points above 1500 K. Electromagnetically levitatable elements which have melting points between 1500 K and 2300 K and are difficult to levitate in a one gravity field include manganese (T_m = 1514 K), silicon (1683 K), and thorium (1964 K). Other elements in this melting point range, which have been studied by levitation, include Be (1551 K), Co (1768 K), Fe (1809 K), Gd (1585 K) to Yb (1700 K) rare earths, Ni (1726 K), Pd (1825 K), Sc (1812 K), Ti (1943 K), V (1710 K), and Y (1768 K). See Bonnell, et al [1985] for a recent review of the status of most of these latter elements.

It is interesting to note that liquid data for the gadolinium to ytterbium higher melting rare earths have not been mentioned widely in the literature [but see Pankratz et al, 1962, 1963; and Robie, et al, 1979], and thus what problems might occur with their levitation are uncertain. However, cerium [Krantz and Bautista, 1976], praseodymium [Stretz and Bautista, 1976], and neodymium [Stretz and Bautista, 1975], have been studied by levitation, thus the ground-based problems should be readily solvable.

Scandium should be similar to titanium and presents significant problems in atmosphere control due to its ready tendency to form the oxide. Lack of measurements are probably due to the expense of the metal and the fact that most current uses are of the oxide. Its future potential as a very light metal

with a higher melting point than aluminium could put it into the same class as titanium as an alloying material. Since no obvious barrier to ground-based studies seems to exist, this material should be attempted on the ground first.

Of the elements listed above as difficult or without reports of successful levitation, thorium's melting point is at the upper end of the range available, which requires complete functioning of the apparatus to insure obtaining liquid data. It is also somewhat radioactive, increasing the on-board risk slightly in case of a catastrophic system failure. Since thorium should be levitatable on earth with precautions, it too should be attempted in a ground environment first.

Manganese is a strategic material, considered to be the single most important additive in the steelmaking process, where about 90% of the total manganese consumed in the U.S. is used [Critical Materials Requirements of the U.S. Steel Industry, 1983]. The pure metal is prepared by electrodeposition, and is obtainable in only thin (> 0.2 cm) platelets, which cannot be consolidated even by arc melting. The material is extremely brittle and has not been levitated electromagnetically due to its unavailability in reasonable bulk form. Although some older thermochemical data have been reported [cf. Metals Handbook, 1976], this element would appear to be a good candidate for a microgravity investigation.

Silicon is a semiconductor, and does not achieve metallic conductivities sufficient to levitate until heated near its melting temperature. The obvious importance of this element to the semiconductor industry, its extreme reactivity, which would make containerless studies very advantageous, and the estimates that it has the largest heat of fusion (ca 60 kJ/mol) of any element make it the most attractive candidate for initial high temperature microgravity

experiments. Its melting point is comparable to that of Be, which has already been levitated by the GE SPAR levitator [Wouch, et al, 1978], which makes a successful first flight experiment likely. Emissivity data are available to above the melting point, so temperature measurement should not present abnormal problems. Combining flight experiments with ground-based studies of the volume change on melting and liquid density of silicon and/or berylium appears to be an attractive initial effort. The results of the GE-RICE-NBS interaction in the recent past make it clear that a successful flight experimental program will need the support of a strong ground-based parallel effort to attract and support personnel, and to provide the continuity of effort necessary to conserve expertise during the flux of students typical of academic research.

Studies of alloys, particularly of extreme refractory systems in composition regions where the liquidus is within the capabilities of the flight apparatus, are also attractive candidates when multiple sample handling capability has been demonstrated. Since a number of specimens of varying composition would be necessary to establish trends, these efforts should follow the initial demonstration types of experiments. Detailed information on density and Cp variations should be quite interesting. Our analysis [Bonnell, et al, 1985] of the cerium-copper alloy system data of Dokko and Bautista [1980] points out the failure of the simple mole fraction estimations generally used for alloys.

During the March 1985 discussions at RICE, the possibility of processing specimens as part of the experimental program was discussed. Gas/condensed phase reactions are generally straightforward to accomplish in the containerless environment, with the general limitation that the product remain a liquid (or near the liquidus) and be a good conductor during the processing. The liquid

limitation is due to the typically strong decrease in gas diffusivity in solids much below their melting point, which halts the reaction upon solidification. The usual method of using powdered solid to increase surface area and minimize diffusion distances requires a container, as to the extent the powder couples with the RF field of the levitation coil, each individual particle will be electrostatically repelled from its neighbors, with the result that any sample not strongly compacted will be dispersed by the RF field.

Gas-liquid high temperature reactions have significant advantages in the electromagnetic containerless environment when compared to reactions in a containter. Electromagnetic stirring provides a much more rapid mixing process near the surface than simple diffusion, and the entire surface of the sample is available to the reactant without stirrer or wall reactions to consider. The introduced gas can be metered into the reaction environment without unwanted reactions through cool nozzles, allowing accurate mass balance determinations, and controlled reaction rates, in contrast to sealed tube type syntheses. In addition, reaction products can be either volatile or non-volatile, or both, and can be separated during the reaction process.

Groups of substances to prepare and make density or Cp measurements similar to those described above for the metallic elements include the oxides, nitrides, and phosphides of conducting elements. In these systems, the stepwise addition of a reactant gas (e.g., oxygen) to the atmosphere surrounding a levitated liquid allows the direct reaction product to be formed. Previous work [Margrave, et al, 1971, Bonnell, et al, 1969] notes that reactions are generally simple, tending to yield the stable product of lowest oxidation state due to the effective excess of metal at the reaction interface. At

higher temperatures, carbides are also quite interesting, but their exceptionally high melting points and the fact that many metal carbides are good electrical conductors makes these syntheses better candidates for a parallel ground-based program. Of the metals which can be melted in expected flight apparatus, the following compounds should be readily synthesized, with volume change measurements used to track extent of reaction, and perhaps cooling-curve thermal measurements possible. Boric oxide (B_2O_3) is a possible first material. Its liquidus properties are reasonably well known [JANAF, 1971; Robie, et al, 1979], and it has the useful property that the liquid oxide is considerably lower melting (723 K) than the metal (2077 K). Of the metals suggested as potentials for early flight experiments, the manganese-oxygen system is very interesting. There are a number of manganese oxides, ranging from MnO (T_m 2058 K) to Mn_3O_4 (1863 K - this transition is dependent on oxygen pressure, being from 1873 K at 1 atm $P(O_2)$, to 1828 K at 0.1 atm $P(O_2)$ - see Driessens [1967] and the commentary in Phase Diagrams for Ceramists [1975, fig. 4157]). The tendency of levitation syntnesis to lead to the lower oxide should allow a natural progression in this system. The phase diagram of the manganese-oxygen system is similar to that of the Fe-O system in complexity, and appears to need more work to permit displaying the detail known in the Fe-O system. Manganese oxides also exhibit compound non-stoicometry around the MnO composition which containerless preparation could investigate. Parallel experiments on the better known Fe-O system (from the Wustite $Fe_{0.947}O$ (T_m = 1652 K) to Fe_2O_3 (1895 K)) might also be in order, either as preparation for studies of the Mn-O system, or as followup in the event containerless processing of oxides proves exceptionally fruitful.

Other oxides which could be considered include silica (T_m = 1996 K) and

oxides of vanadium, which has stable solids of compositions VO (T_m = 2350 K), V_2O_3 (2240 K), V_3O_5 (2100 K), VO_2 (1818 K), V_2O_5 (943 K) and Y_2O_3. The Y-O system is particularly attractive if the available temperature range becomes higher, because of the interest in oxide film corrosion protection by yttrium in superalloys. Also, in general, the sesquioxides of the lanthanides exhibit solid polymorphism. If these oxides can be prepared, and solidified in the high temperature polymorph, due to lack of external nucleation sites, new insight into high temperature behavior could result.

Toropov, et al [1972] note that the first three ionization potentials of Sc, Y, and La are low so that they can give up two electrons for the formation of oxygen bonds, while the third electron is a conductivity band electron. Thus ScO and YO may exhibit metallic conductivity, particularly at elevated temperatures. This possibility certainly makes these oxides excellent ground base test case possibilities, and should be excellent choices for determining the limits of electromagnetic positioning of compounds. This information will be necessary to determine if alternate heating will be required during syntheses.

The major result of these experiments, however, would be the actual processed specimens, including the probability of large crystalline specimens, for chemical characterization and microstructural comparison of the containerless prepared material with conventional materials. This pioneering work should provide important scientific guidance for the use of the microgravity containerless environment as a tool in the synthetic chemist's arsenal for tailoring materials.

Liquid Tungsten

Previous work on this project yielded the first levitation measurement

of the heat of fusion of tungsten [cf. Bonnell, 1983, Bonnell, 1984]. The value, 53.0 ± 2.3 kJ/mol, was obtained by analysis of fraction melted versus heat content data from drop calorimetry of the specimens. Continued efforts to obtain Cp data on the levitated liquid has proved fruitless, as the available generator power at GE was apparently insufficient to provide stable liquid levitation. Recently, German workers [Arpaci and Frohberg, 1984], utilized a 50 kW, 900 kHz induction heater to obtain enthalpy increment data for tungsten liquid and solid. Although those authors unfortunately give no details of the coil design, the use of higher power solved the difficulties in levitating molten tungsten, as they reported 20 measurements of the liquid over the temperature span from 3699 K to 4017 K, with an average deviation of 0.42 %, which is indicative of excellent high temperature measurements. Arpaci and Frohberg obtained the heat of fusion directly from the difference of their solid data as 50.3 ± 0.4 kJ/mol at 3683 K. They apparently did not directly determine the melting temperature, but used the commonly referenced literature value 3683 K to determine emissivities and establish their temperature scale. This value and other literature on the melting temperature of tungsten have been reviewed by Cezairliyan [1972] and a recommended value of 3695 K was selected in light of improvements in measurement methodology. Using this temperature (3695 K), the Arpaci and Frohberg [1984] heat of fusion, ΔH_m, changes insignificantly (to 50.4 ± 0.4 kJ/mol), relative to the solid value from their fitted equation of 118.7 (± 0.3) kJ/mol at 3695 K. Our analysis of our heat of fusion determinations gave the value, 119.5 ± 2 kJ, for the solid independently, which is also in nearly exact agreement with JANAF [1971]. Arpaci and Frohberg considered the literature of solid tungsten carefully, and noted positive deviations in the recent literature of over 4%. Comparing

solid enthalpy values shows our derived solid value to be within 0.6% of the Arpaci and Frohberg value, and well within the combined error limits. Because our value of the heat of fusion is independent of literature solid data, and references a solid value in good agreement with the Arpaci and Frohberg value, the two studies can be directly compared, and the agreement is quite good, considering that in both cases, differences in rather large numbers are involved. Arpaci and Frohberg do not state where they derive their error estimate for ΔH_m, but apparently, using the difference fit $H(\ell,T) = H(\ell,T_m) + Cp \times (T - T_m)$ they have accepted the error in the intercept term as the error in ΔH_m. Refitting the data of their Table 2 indicates a standard error for the fit of 888 J, in line with what would be expected from an average deviation of 0.42% for ca 170 kJ/mol. Combined with the 298 J error estimate from the solid data gives an error estimate for ΔH_m of at least 600 J/mol. The better error estimate should be to use the larger uncertainty. Alternatively, combining the uncertainty of the solid with the intercept error suggests an uncertainty of 670 J/mol. It is suggested that the uncertainty is better represented by a value of at least ± 0.8 kJ/mol. The agreement between the calorimetric heats of fusion [Arpaci and Frohberg, 1985; Bonnell, 1984] is within 1.5% of the total heat, which is excellent agreement for difference measurements.

Although a ΔH_m of 51 kJ is higher than the Tamman rule [1913] estimate by nearly 70 percent, this value is in accord with periodic correlation estimates which indicate that the entropy of melting, ΔS_m, should be somewhat higher than the fusion entropy for molybdenum (12.9 J/mol·K). Our work [Bonnell, 1983, 1984] gives ΔS_m = 14.3 ± 0.6 J/mol·K, in reasonable agreement with the value of Arpaci and Frohberg [1984], corrected to a 3695 K melting point, of

13.6 ± 0.2 J/mol.K. Using an error-weighted average of the two values for ΔS_m gives a best value of 13.8 ± 0.3 J/mol.K. The entropy of fusion of tungsten is thus 7% larger than molybdenum.

With two independent calorimetric studies in good agreement, it appears that the melting thermodynamic properties of tungsten are now reasonably well known. The coincidence of the heats of fusion also indicate that the emissivity values used by Arpaci and Frohberg, and their derived heat capacity of the liquid are reliable.

Prototype Data Acquisition and Analysis

The advent of "personal" computers with the capability of supporting high level languages, and with a relative ease of being transported suggested that it was an appropriate time to consider a computer-based acquisition system which could be brought to the experimental site along with the rest of the apparatus. Previous experimental efforts had developed a datalogging system, which could be used via a telephone link to the NBS computer system to reduce calorimetric data. The relatively slow speed and unreliability of transmission for this work has been a general problem area. The large calorimeter used in this work requires about 1 hour to reach steady state after an impulse change. In order to provide for more than one run in a day, it was necessary to wait until the end of the day to process data, so the second and succeeding run of the day could not be planned on the basis of the previous runs. With a large number of aborted drops, it would be desirable to be able to analyze the drift rate of the calorimeter in an ongoing fashion to determine when the calorimeter was ready.

The data reduction program, CALOR, is written in FORTRAN, and during this effort, was converted to ANSI FORTRAN 77 running on the NBS mainframe

Sperry 1100/82. Among other changes, this involved replacing the character manipulation performed for report generation originally implemented in integer data types with true character data types, adding new code to permit CALOR to recognize and process a variety of input stream formats, and other minor code cleanups. The program is, however, by nature, a batch program, and requires multiple runs to determine such data characteristics as the end of the main period and whether a portion of a drift period is linear, even though the data stream collected may exhibit curvature. Once these characteristics are determined, its reporting facilities are excellent. A real-time control and report program actually has different goals than the final data reduction program, and a reasonable way to approach the problem was to develop two codes, one for the run-time acquisition and monitoring process, and one for final data reduction, both to run from files created on the portable computer system.

For this purpose, NBS has procured a transportable computer system, compatable with the IBM* Personal Computer type of system. The Corona* PCC-2 portable was chosen because of its ability to be maximally configured (2 5-1/4" floppy disk drives, 512 kBytes memory, 9 in. internal monitor with ultra-high resolution text display, serial and parallel ports, full size, enhanced function keyboard, etc.) and leave expansion slot space for a full size modem card, a data acquisition card, and a battery backed-up clock card. Although other vendors (with restricted choices of add-ins) can now meet many of these requirements, that was not the case when the computer was procured. The advantage of IBM PC compatability is the large number of languages, e.g., FORTRAN 77, BASIC, PASCAL, APL, C. FORTH, etc., available in implementations

---

* Mention of products by brand name is to provide identification of a commercially obtained or evaluated item, and is not to be construed as Government endorsement or certification of suitability for other applications.

likely to be portable across a variety of different machine configurations.

The availability of FORTRAN 77 for the compilation of CALOR has proved to be more problematical than expected. Until recently, no full language FORTRAN 77 compiler was available for the IBM PC, running under MS-DOS, the overwhelmingly accepted operating system. Of the subset compilers, Microsoft FORTRAN has received the best reviews, particularly for both code quality and freedom from bugs. However, the implementation tested, version 3.20, evidenced a number of missing features and implementation bugs which required major revision of portions of the character manipulation code. As examples, only one length character variable can be typed in a statement; attempts to use *n designators resulted in undefined objects; character concatenation is not supported, nor are substring operations; character type variables cannot be intermixed with numeric types in COMMON. Considering the amount of debugging necessary to overcome these problems, and the fact that the resulting code would be somewhat specific to the compiler, it was decided to delay this implementation until one of the new full languages compilers was released. Two compilers are under consideration: Digital Research* (DR) FORTRAN 77 and the IBM/Ryan-McFarland* Professional FORTRAN. The DR FORTRAN, although a full language compiler, was reviewed by NBS [Kahaner, 1985] for use and found to have so many bugs that its use was not recommended. Some preliminary testing has been undertaken on the Professional FORTRAN compiler by the NBS Scientific Computing Division with highly positive results. They could find no significant problems and so far have found it to be a complete full language implementation. The processor fully supports current levels of MS-DOS (i.e., versions 2.1 and 3.0) and can access files at any tree depth. However, delivery of the processor from IBM has been slow, and a copy for this project was received too late to complete the port of CALOR to the PC in this reporting period.

For the data control portion of the project, a number of factors were considered. Primary was the selection of a language which was interactive and portable, handled serial I/O well, and provided a powerful and flexible development environment, since the actual algorithms to provide real-time support to the experimentalist must be developed piecemeal, with considerable testing against recorded as well as actual datasets. The languages considered as meeting the interactive requirement and the wide use necessary to assure portability were BASIC, APL, and FORTH. FORTH still lacks a standard method for handling floating point and would require extended programming expertise for its users until the control system was stable. It was felt after examination of the FORTH language that it was the most powerful and flexible for control codes, but that algorithm development would be quite difficult and protracted for this project.

BASIC was rejected, as the defacto standard Microsoft BASIC makes modular development extremely difficult. Its lack of local parameters, the lack of support for passed parameters to subroutines, its lack of support for the 8087 math co-processor, and its restriction to the small (< 64 kByte) memory model all mitigate against the language. In its favor is the fact that much microcomputer assembly language support code for data acquisition devices is compatable with the BASIC CALL statement. Also, with restrictions, interpreter BASIC code can be compiled with the BASIC compiler for major execution improvements, but with the disadvantages of compilation. However the compiler, and the interpreter until very recently, have been unable to utilize the MS-DOS 2.0 level tree structured file system, thus further limiting the capabilities of BASIC. Although it is perfectly possible to write extremely sophisticated systems in BASIC, maintenance of the code generally requires the

author's support. It appears that so much code is written in BASIC because of its simplicity, its similarity to FORTRAN syntax, the advantages of interpreter debugging, the universal availability of similar versions of the language on microcomputers, and until very recently the lack of alternate languages.

The advent of low cost semiconductor memory and microprocessors which can address large extents of memory (e.g., 512 kByte or more), has made the availability of another interactive language possible. Although APL requires considerable memory for the processor alone (~192 kB) and the manipulations of APL can be memory intensive, the parallel nature of the language permits execution speeds often approaching that of compiled language when handling quantities of data. For example, with an 8087 coprocessor, APL sums vectors of 1000 double precision values in ~100 ms. Least square fit of a linear model to 60 data points requires <2 s. The sum in GW BASIC requires over 8 seconds, and is in error in the 10 decimal place due to improper conversion of decimal numbers to double precision. Calorimetric data reduction requires linear estimation, numeric integration, and running differences calculations, all of which require double precision arithmetic and fast execution. These computations are simple code in APL in contrast to BASIC.

Algorithms in APL are generally totally portable where file I/O is not involved. The modularity of the language permits that non-portability to be localized easily. Scientific Time Sharing Corporation* (STSC), one of the major sources of mainframe APL, has made a strong entry into the microcomputer market by releasing a complete implementation of their mainframe processor, APL*PLUS, for IBM and compatable PC's. The supported environment is superior to mainframe usage, and is comparable in flexibility to the best FORTH

environments. The majority of algorithm development required is quite suited to the vector capabilities of APL, particularly the least square fitting of the initial and final period processes, and the integration of the main period data. Although less accepted than BASIC, the clear superiority of APL over BASIC makes it the preferred choice for the interactive calorimetric system prototyping.

Specific interactive code development will be begun as soon as the porting of the data reduction code, CALOR, is complete.

References

1. Arpaci, A. and Frohberg, G., Z. Metallkde. 75, 614-618 (1984).

2. Bonnell, D. W., Chauduri, A. K., and Margrave, J. L., unpublished work (1969).

3. Bonnell, D. W. and Margrave, J. L., unpublished work, Rice University (1974).

4. Bonnell, D. W., NBS: Materials Measurements, ed. J. R. Manning, NBSIR-82-2560, p. 83-103 (1982).

5. Bonnell, D. W., NBS: Materials Measurements, ed. J. R. Manning, NBSIR-83-2772, p. 113-130 (1983).

6. Bonnell, D. W., NBS: Materials Measurementd, ed. J. R. Manning, NBSIR-84-2882, p. 135-152 (1984).

7. Bonnell, D. W. Montgomery R. L., Stephenson, B., Sundareswaren, P. C., and Margrave, J. L., in Heat Capacity of Solids, ed. A. Cezairliyan, McGraw-Hill, (1985 in press).

8. Critical Materials Requirements of the U.S. Steel Industry, (prepared under the National Materials and Minerals Policy Research and Development Act of 1980, Dept. of Commerce, March 1983).

9. Cezairliyan, A., High Temp. Sci., 4, 248 (1972).

10. Dokko, W. and Bautista, R. G., Met. Trans. B 11, 511-18 (1980).

11. Doremus, R., Informal Report to R. Halpern, NASA Headquarters, April 5, 1985.

12. Driessens, F. C. M., Inorg. Chim. Acta, 1, 193 (1967).

13. Frost, R. T. and Stockoff, E., Final Report, NASA Contract NAS8-34231, Task 7 (GE Space Systems Division, Valley Forge, PA, 1983).

14. Frost, R. T., private communication, February 1985.

15. JANAF ThermoChemical Tables, 2nd Edition, ed. D. R. Stull, H. Prophet, et al, NSRDS-NBS 37 (U.S. Govt. Printing Office, 1971), and supplements 1974-1982.

16. Kahaner, D., (NBS-Scientific Computing Division), private communication, 1985.

17. Kuntz, L. L. and Bautista, R. G., Met. Trans. B7, 107-113 (1976).

18. Margrave, J. L., Treverton, J. A., and Wilson, P. W., High Temp. Sci., 3, 163-167 (1971).

19. Metals Reference Book, Fifth Edition, ed. C. J. Smithells and E. A. Brandes, (Butterworths, London and Boston, 1976, p. 944).

20. Pankratz, L. B., King, E. G., and Kelley, K. K., U.S. Bureau Mines Rept. Inv. 6033 (1962).

21. Pankratz, L. B. and King, E. G., U.S. Bureau Mines Rept. Inv. 6175 (1963).

22. Phase Diagrams for Ceramists, 1975 supplement, ed. Levin and McMurdie, (Amer. Ceram. Soc., Columbus, OH, 1975).

23. Robie, R. A., Hemingway, B. S., and Fisher, J. R., U.S. Geological Survey Bulletin 1452 (U.S. Govt. Printing Office, Washington, DC, 1979).

24. Stretz, L. A. and Bautista, R. G., High Temp. Sci., 7, 197-203 (1975).

25. Stretz, L. A. and Bautista, R. G., J. Chem. Eng. Data 21, 13-15 (1976).

26. Toropov, N. A., Barzakovskii, V. P., Bondar, I. A., and Udalov, Yu. P., Handbook of Phase Diagrams of Silicate Systems, Vol. II Metal-Oxygen Compounds in Silicate Systems (Translation U.S. Dept. of Commerce, NTIS, Springfield, VA, 1972).

27. Weingarten, J., Bonnell, D. W., and Margrave, J. L., "Thermodynamic Property Determination in Low Gravity," Final Report, NASA Contract NAS8-32030 (1977).

28. Wouch, G., Grey, E. L., Frost, R. L., and Lord, A. E., Jr., High Temp. Sci., 10, 241 (1978).